Master's Programme in Chemical and Process Engineering

A Study on Optimization of Graphite Separation in Lithium-ion Battery Waste Recycling via Froth Flotation and Selective Flocculation: A Response Surface Methodology Approach

Sevda Dilmaghani

Supervisor **Associate Professor Rodrigo Serna-Guerrero**

Advisors **Dr. Natalia Araya Gómez**
M.Sc. Mohazzam Saeed

Master's thesis
July 2024

Aalto-yliopisto
Aalto-universitetet
Aalto University

Author Sevda Dilmaghani

Title of thesis A Study on Optimization of Graphite Separation in Lithium-ion Battery Waste Recycling via Froth Flotation and Selective Flocculation: A Response Surface Methodology Approach

Programme Master's Programme in Chemical, Biochemical and Material Engineering

Major Chemical and Process Engineering

Thesis supervisor Associate Professor Rodrigo Serna-Guerrero

Thesis advisor(s) Dr Natalia Araya Gómez, and MSc Mohazzam Saeed

Date 30.07.2024 **Number of pages** 67+2 **Language** English

Abstract

The growing demand for lithium-ion batteries (LIBs) necessitates effective recycling methods to recover valuable materials and mitigate environmental impact. This study investigates the optimization of graphite separation from LIB waste using froth flotation and selective flocculation. Flotation is utilized due to the natural hydrophobicity of graphite compared to the hydrophilic nature of cathode materials, making it a suitable method for separation. Selective flocculation is explored to enhance the efficiency of this process by promoting the aggregation of target particles.

Key flotation parameters, including solid content, impeller tip speed, conditioning time, and flocculant dosage, were systematically varied and analyzed using a Response Surface Methodology (RSM) approach. Results indicated that employing ultrafine cathode particles (<10 μm) in the model black mass feed achieved a graphite concentrate grade of 98.63% with a recovery rate of 71.98% in a single-stage flotation process. Among the parameters studied, solid content was found to have the most significant impact on graphite grade, while impeller tip speed and flocculant dosage most influenced graphite recovery.

Through response optimization, it was determined that optimal conditions include a solid content of 20 g/L, a conditioning time of 13 min, and an impeller tip speed of 1040 rpm, resulting in a graphite grade of 99.02% and a graphite recovery of 74.54%. This study highlights the potential of combining froth flotation with RSM to enhance the efficiency and effectiveness of graphite separation in LIB recycling processes. Future research should explore alternative pH levels, flocculants, and multi-stage flotation processes to further improve separation performance.

Keywords Graphite Separation, Lithium-ion Battery Recycling, Froth Flotation, Selective Flocculation, Design of Experiment, Response Surface Methodology, Recycling Optimization, Flotation Parameters, Model Black Mass

Table of Contents

Preface and Acknowledgements

During the early stages of my studies, I was exploring different fields to discover which one truly inspired me. Thanks to Professor Rodrigo Serna and Gulsah Tas, I joined the Mineral Processing and Recycling research group at Aalto University. This experience was a turning point in my professional life, as I found my passion for sustainable battery recycling.

In February 2024, I rejoined the team to work on my thesis. I am deeply grateful to Professor Rodrigo Serna for the opportunity to write my thesis under his supervision. His support, along with the invaluable guidance from my advisors Natalia Araya Gómez, and Mohazzam Saeed has been instrumental in making this project possible. I appreciate their patience and encouragement throughout this process. I also wish to extend my sincere appreciation to Tommi Rinne for his significant contributions and assistance.

I am thankful to all members of the Mineral Processing and Recycling group for their kindness and support. Special thanks to Gulsah Tas, Luis Gomez, and Hanna Sahivirta for their help with this project.

Furthermore, I am grateful to my family—my supportive father, caring mother, and lovely sisters, Sara and Saharnaz—for their unwavering love and support. I also want to thank Saharnaz and Alireza, who have been my role models. I appreciate my dear uncle Jafarsadegh for all his support and valuable suggestions. None of this would have been possible without their care and encouragement.

My heartfelt thanks also go to my dear friends Zeynab F., Fatemeh P., Reyhane F., Fatemeh F., Sadegh C., Amir Mohammad G., Maryam M., and Masoud T. for always being there for me and making this journey memorable.

Lastly, a special thanks to Kristian for showing me the beauty of Finland and bringing peace and joy into my life. His support and encouragement have been a cherished part of this journey.

Cheers,

Helsinki, Finland
July 2024

Sevda Dilmaghani

List of Tables

List of Figures

1 Introduction

1.1 The Societal and Economic Importance of Lithium-ion Batteries

Lithium-ion batteries (LIB) are one of the most important electrochemical energy storage devices, powering electronic mobile devices and electric vehicles alike (Velázquez-Martínez et al., 2019). However, there is a remarkable difference between their rate of production and recycling (Velázquez-Martínez et al., 2019). Growing global demands for raw materials used in manufacturing LIBs, such as Co, Mn, Ni, Li, and graphite, have further stressed their already scarce supply (Olivetti et al., 2017). Figure 1 illustrates the growing global demand for LIBs by 2023, with a significant increase observed particularly in Europe.

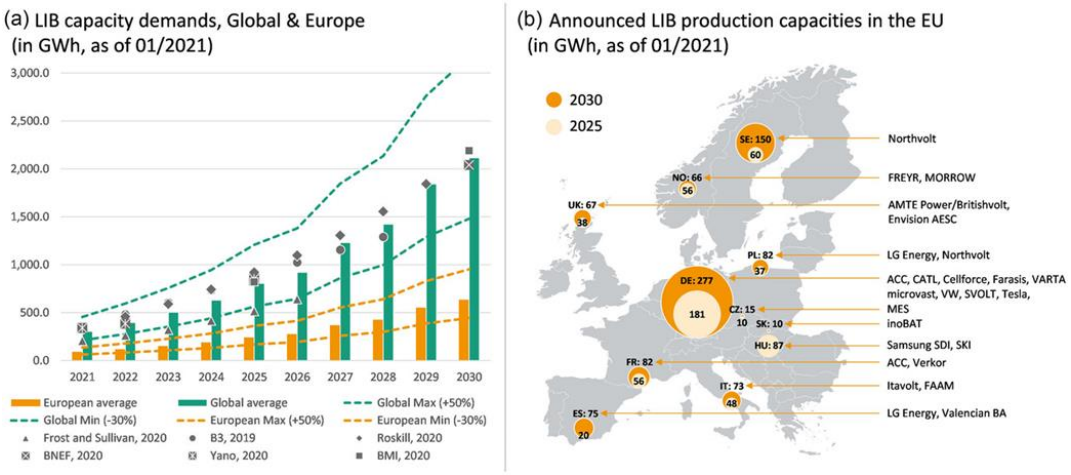

Figure 1 (a) Lithium-ion battery (LIB) capacity demands globally and in Europe. (b) Announced cell production capacities in the European Union (EU) (Hettesheimer et al., 2021).

The data shown are from a meta-study conducted by the Fraunhofer Institute for Systems and Innovation Research ISI, which uses forecasts and market studies from various market forecast companies (B3, Benchmark Mineral Intelligence, BloombergNEF, Frost & Sullivan, Roskill, Yano Research Institute). Global battery cell production is expected to grow to 2000 GWh/a by 2030, with a minimum scenario of 1500 GWh/a and a maximum scenario of 3200 GWh/a. A large part of the demand is solely to produce battery cells for EVs (Hettesheimer et al., 2021). For Europe, production volumes of approximately 984 GWh/a by 2030 have already been announced (Hettesheimer et al., 2021). However, it must be considered that not all announced projects will be realized until 2030 (Degen, 2023). Nevertheless, by 2030, the battery

cell market will increase significantly. This is a significant challenge for the European Union (EU), which aims to reduce greenhouse gas (GHG) emissions significantly by 2030 (EuropeanCommission, 2021a). On the one hand, EVs support this goal, but on the other hand, LIB production is a new, growing market with significant energy consumption and GHG emissions (Romare & Dahllöf, 2017). Therefore, European Commission plans to regulate this market, with respect to its ecological aspects, and mandate an ecological battery passport by 2026 (EuropeanCommission, 2020). Efficient recycling of LIBs can significantly reduce the overall GHG emissions associated with battery production and is a crucial economic and socio-political issue for sustainable development.

1.2 Challenges in LIBs Recycling

Given the exponential increase in the production of lithium-ion batteries (LIBs) used in electric cars and the sizeable quantity of waste produced at the end of their lifespans, efficient recycling of used lithium-ion batteries offers tremendous promise for practical application (Shang et al., 2024). While considerable efforts have been devoted to recycling cathode materials and other valuable components in spent lithium-ion batteries, sufficient attention has not been directed towards the spent anode graphite (Shang et al., 2024).

Graphite has been the predominant anode material in commercial LIBs due to its safety, reliability, low cost, stable operating potential, and satisfactory energy density. LIBs generally include 12 to 21 wt.% graphite and approximately 15% of the cost of the LIBs depending on the type of battery (Y. Wang et al., 2021). One electric hybrid car contains about 10 kg of graphite, while a fully electric vehicle contains around 50 kg of graphite (Shang et al., 2024). According to the anticipated new energy vehicle sales volume in China, the demand for battery-grade graphite will be about 101 million tons in 2025 and 285 million tons in 2035, respectively (Natarajan & Aravindan, 2020; Zhang et al., 2024)

In addition, the 2023 European Critical Raw Materials Regulation have categorized active materials for LIBs, namely Co, Ni, Li, Mn, and graphite, as strategic raw materials, owing to their significance in the realm of green technology, and their inherent potential to pose supply chain vulnerabilities in the future (EuropeanCommission, 2023b). Among the strategic raw materials essential for LIBs, graphite is the only non-recoverable material in current industrial LIB recycling methodologies, hydrometallurgy and pyrometallurgy (Beaudet et al., 2020). Therefore, it is anticipated that the recycling of battery-grade graphite will gain significance in the upcoming years.

In industrial LIB recycling processes, end-of-life batteries are processed mechanically to separate the active components into a fine powder mixture commonly known as “black mass” (Harper et al., 2019). The cathode oxides are commonly hydrophilic, whereas graphite is a naturally hydrophobic mineral (Rinne et al., 2024). Due to this wettability gradient, flotation is a promising technology for separating graphite, and it has been studied by several authors as a potential separation process for the cathode and anode powders (Dańczak et al., 2021; Folayan et al., 2021; Hong et al., 2024; Li et al., 2021; Liu et al., 2020; Nazari et al., 2024; Ruismäki et al., 2020; Salces et al., 2022; Saneie et al., 2022; Vanderbruggen, Sygusch, et al., 2021; C. Wang et al., 2023; Wang & Liu, 2024)

Rinne et al. (2023) investigated the selective flocculation of model black mass and proposed that this technique is a promising method to improve the recycling rate of spent LIBs and achieve circularity for battery grade graphite.

Additionally, a significant challenge in flotation selectivity is the imperfect liberation of the active particles. Organic binders that coat electrode particles often cause difficulties in liberating and extracting these materials (Fu et al., 2021). Most research on black mass flotation has focused on the preprocessing to improve particle liberation, specifically targeting the degradation of binder materials that hinder the separation (Traore & Kelebek, 2023). Wei et al. (2023) reported that the challenge of completely removing binders from cathodes leads to approximately 10% of cathode materials ending up in the froth graphite products, causing a significant loss of valuable cathode materials.

Addressing these challenges is crucial for advancing LIB recycling technologies. Continued research into improving the efficiency and effectiveness of separation processes, such as flotation, and optimizing preprocessing methods will be essential for developing more sustainable and economically viable recycling solutions.

1.3 Research Question

The research question of this study can be summarized as:

How different operating parameters, including solid content, impeller tip speed, conditioning time, and flocculant dosage, affect the performance of flotation in optimizing graphite separation from synthetic black mass. This research aims to understand the influence of these parameters on graphite grade and recovery. By systematically analyzing these factors, the study seeks to identify the optimal conditions for maximizing graphite recovery and purity in the flotation process.

2 Background

In this chapter, the structure of lithium-ion batteries is explained. Subsequently, froth flotation and selective flocculation are described as emerging techniques for the beneficiation of the fine fraction of the black mass. Additionally, the design of experiment, process analysis and evaluation tools used in this research are presented.

2.1 Structure of a Lithium-ion Battery

Recycling processes aim to separate and recover active material. Understanding the structure of LIB is crucial for recognizing the challenges faced in their separation (Vanderbruggen, 2022). Figure 2 indicates the details of a lithium-ion battery.

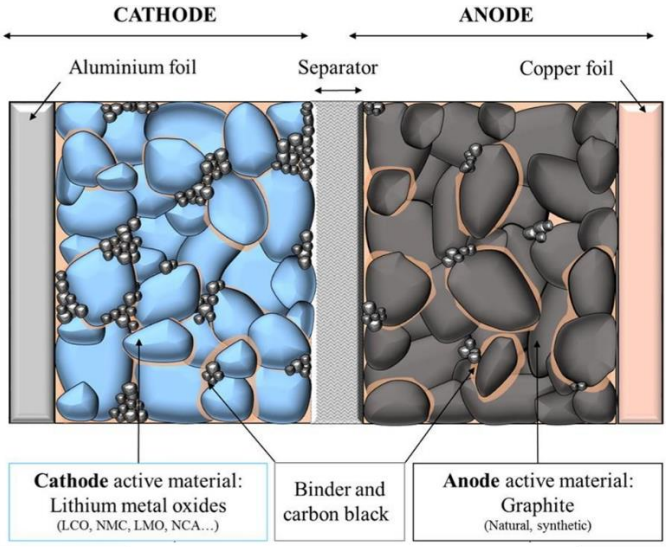

Figure 2 Details of a Lithium-ion battery. Adapted from Vanderbruggen et al., (2021a).

Generally, a LIB is composed of a cathode, an anode, and a separator, which are immersed in the liquid electrolyte and sealed in the stainless steel, aluminum case or plastic pouch. The anode contains graphite powder as the active material, which is mixed with a binder, typically polyvinylidene fluoride (PVDF), and coated on a Cu foil current collector. On the other hand, the cathode may comprise different type of active materials, including lithium metal oxides or phosphides, such as $LiCoO_2$ (LCO), $LiMn_2O_4$ (LMO), $LiNi_xCo_yMn_zO_2$ (LNCM), $LiNi_xCo_yAl_zO_2$ (LNCA), and $LiFePO_4$ (LFP), which are coated on an Al current collector with carbon black as the conducting agent and PVDF as the binder (Nazari et al., 2024; Y. Wang et al., 2021).(Tarascon & Armand, 2001)

The migration of lithium ions from the LCO cathode to the graphite anode (discharge process) or vice versa (charge process) could be used to explain the mechanism of energy conversion in these batteries. This process is expressed in Equation 1 (Zhang et al., 1998).

$$LiCoO_2 + 6C \leftrightarrow Li(1\text{-}x)CoO_2 + C_6Li_x \quad (1)$$

In the context of LIBs recycling, froth flotation can be used to separate valuable cathode materials (such as LCO, NMC, and LMO) from other cathode materials, as well as to separate graphite from other anode materials (Nazari et al., 2024).

The cathode active materials are strongly adhered to the Al current collector by the binder, making it difficult to separate the binder from the active material. As a result, industrial waste LIB active materials are often coated with residual binder polymers, which can alter the surface properties of the active material. Since binder removal was beyond the scope of this study, a model black mass was utilized.

2.2 Principle of Flotation

Flotation is a separation process that exploits natural and induced differences in the surface wettability of minerals. It distinguishes between minerals that are readily wetted by water (hydrophilic) and those that repel water (hydrophobic) (Wills & Finch, 2015). As shown in Figure 3, the hydrophobic mineral particles attach to air bubbles, causing these minerals to float to the surface of the slurry along with the air bubbles (Schlesinger et al., 2022). In conventional flotation, the froth phase contains the target mineral and is referred to as a concentrate. Conversely, hydrophilic particles, known as tailings, sink and accumulate as the bottom product during this process (Kupka, 2020).

In reverse flotation, it is the gangue minerals that are enriched in the froth phase. This process is often employed when the target mineral is hydrophilic and the gangue is hydrophobic. Black mass flotation, which involves separating graphite from lithium-ion battery waste, is more akin to reverse flotation, as graphite is generally less valuable compared to the cathode materials such as lithium-metal oxides (LiMeOs). However, in our study, both minerals are considered valuable, and thus we focus on optimizing the process parameters to achieve a high purity of graphite while maintaining effective separation of the cathode materials. This dual focus necessitates an investigation into the appropriate processes and parameters required to ensure that both graphite and cathode materials meet the desired quality standards.

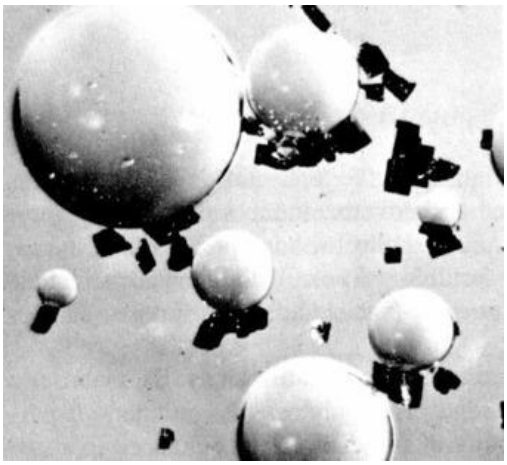

Figure 3 Photograph of water-repellent mineral particles attached to rising bubbles. Photograph by H. Rush Spedden.

Flotation is a complex system, that involves three different phases (solids, liquid, and gas) and the interaction of chemical and physical variables. The chemical variables aim to control the transition between the hydrophilic and hydrophobic states. Physical variables include those resulting from ore properties, such as particle size and composition (liberation), and machine derived factors such as air rate and bubble size (Wills & Finch, 2015). According to Klimpel (1984), the interactions can be presented as a triangle between chemistry, ore and machine.

The process of material being recovered by flotation from pulp comprises three mechanisms (Wills & Finch, 2015):

1. Selective attachment to air bubbles (or 'true flotation')
2. Entrainment in water which passes through the froth.
3. Physical entrapment between particles in the froth attached to air bubbles (often referred to as 'aggregation')

The attachment of valuable minerals to air bubbles is the most crucial mechanism and represents the majority of particles that are recovered to the concentrate. Unlike true flotation, which is selective to the mineral surface properties, gangue and valuable minerals can be recovered by entrainment and entrapment (Wills & Finch, 2015).

Entrainment is a mechanical transfer process by which mineral particles suspended in water enter the froth, move upwards, and finally leave the flotation cell with the mineral particles recovered by true flotation. It plays a critical role especially in the processing of ores with a large proportion of fine gangue particles (Fuerstenau & Fitzgerald, 1989; Kirjavainen, 1996). The quality of

final products in mineral flotation is often greatly influenced by entrained gangue materials (Wang et al., 2016).

Figure 4 illustrates the principle of true flotation in a mechanical flotation cell (Schlesinger et al., 2022). The agitator provides enough turbulence in the pulp phase to promote collision of particles and bubbles, which results in the attachment of hydrophobic particles to bubbles (forming bubble-particle aggregates) and their transport into the froth phase for recovery (Wills & Finch, 2015).

The process can only be applied to relatively fine particles, because if they are too large, either the adhesion between the particle and the bubble will be less than the particle weight and the bubble will therefore drop its load, or the bubble-particle aggregate density will exceed that of the pulp (Wills & Finch, 2015).

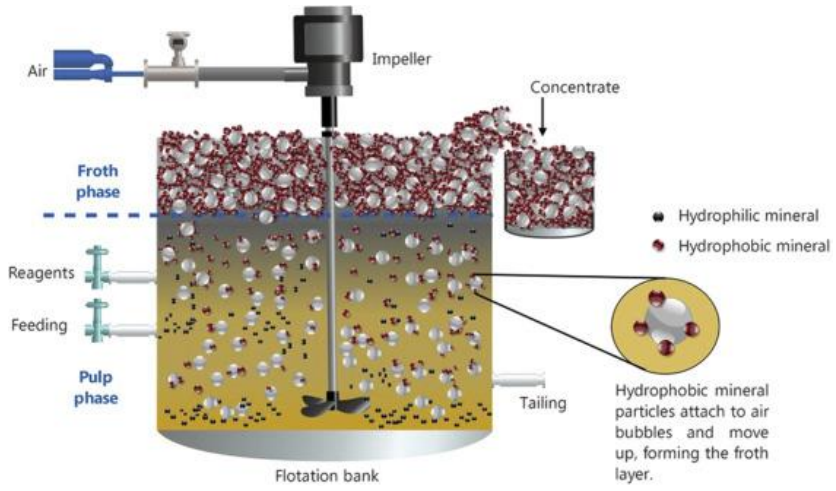

Figure 4 Principle of froth flotation (Schlesinger et al., 2022).

2.3 Flotation Reagents

Flotation reagents are a group of chemicals that are utilized to improve the floatability of minerals. They are roughly divided into four categories: collectors, depressants, regulators, and frothers. In this chapter, only frother and regulators are discussed, as the other reagents are not used in this study.

2.3.1 Frother

Frothers are heteropolar surfactants used in flotation to aid formation and preservation of small bubbles, reduce bubble rise velocity, and form stable froth (Klimpel & Isherwood, 1991). Reduction in bubble size increases the number and total surface area of bubbles, which increases the collision rate with particles and thus increases flotation kinetics. Reducing rise velocity increases the residence time of bubbles in the pulp, increasing the number of

collisions with particles and hence further increasing kinetics. Formation of a froth means the bubbles do not burst when they reach the top of the pulp, which enables the collected particles to overflow as the float product (Wills & Finch, 2015).

Figure 5 presents a general structure of the frother molecule. Most frothers are heteropolar compounds comprising a polar (i.e., hydrophilic) group, typically hydroxyl, and a hydrophobic hydrocarbon chain. The heteropolar structure of the frother molecule leads to its adsorption at the air-water interface, with the nonpolar groups oriented toward the air and the polar groups toward the water (Wills & Finch, 2015).

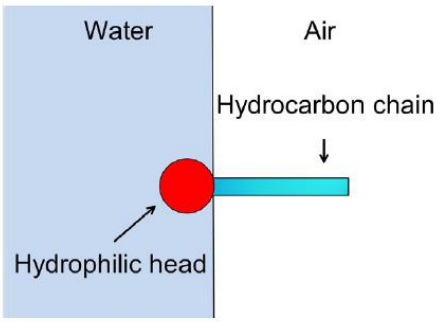

Figure 5 General structure of frother molecule and orientation at the gas-liquid interface (Wills & Finch, 2015).

Among the aliphatic alcohols tested on spent LIBs, methyl isobutyl carbinol (MIBC) proved the most efficient frother (Ahmad & Xu, 2015; Khoshdast et al., 2015; Klimpel, 1995). It is excellent for emulsifying water-oil mixtures because of its hydroxide group (Nazari et al., 2024). In this study, MIBC is also used as the frother.

2.3.2 Regulators

The purpose of regulators or modifiers is to enhance the flotation selectivity by modifying the action of the collector on the mineral surface. These chemicals can be classified as activators, depressants, and pH regulators (Wills & Finch, 2015). Activators alter the chemical nature of mineral surface so that they can react with the collector and become hydrophobic.

Depressants increase the selectivity of flotation by rendering certain minerals hydrophilic, thus preventing their flotation (Wills & Finch, 2015).

Regulating the pH of the pulp is also important in order to achieve a selective hydrophobization of the valuable mineral. In this study, alkalinity is controlled by the addition of sodium hydroxide and hydrochloric acid.

2.4 Selective Flocculation

The industrial black mass contains significant quantities of ultrafine particles, mainly from the cathode active material (Vanderbruggen, Gugala, et al., 2021; Vanderbruggen et al., 2022; Vanderbruggen, Sygusch, et al., 2021). It is generally accepted that flotation performs optimally when separating particles are between 15 µm and 150 µm (Farrokhpay et al., 2021).

Ultrafine particles of <10 µm, however, are more vulnerable to being mechanically entrained in the froth due to fluid drag forces becoming dominant over the hydrophobic/hydrophilic interactions for particles of small mass (C. Wang, C. Sun, & Q. Liu, 2021; C. Wang, P. Wang, et al., 2021). In the context of black mass flotation, this phenomenon increases the non-selective recovery of hydrophilic cathode particles in the froth and lowers the grade of the graphite concentrate, even if the active particles are fully liberated. Therefore, it is hypothesized that excess entrainment needs to be prevented to recover battery-grade graphite from black mass via froth flotation (Rinne et al., 2023).

Flocculation of fine particles using polymeric materials (flocculants) and separating such aggregates from particles of other components in the dispersed phase is known as selective flocculation (Mathur et al., 2000). The competition between different surfaces for the flocculant must be controlled to achieve adsorption on the targeted component. The aggregates of the polymer-coated particles or “flocs” thus formed are separated from the suspension either by sedimentation/elutriation or floc-flotation (Mathur et al., 2000). Provided they are robust enough, the flocs can be further cleaned, to improve the concentrate grade.

The selective flocculation process involves four steps: (1) dispersion of the fine particles (typically dispersants are added at this stage), (2) selective adsorption of the polymer on the flocculating component and formation of the flocs, (3) floc growth which is generally achieved by conditioning at low shear, and (4) floc separation either through sedimentation/elutriation/sieving or flotation (Mathur et al., 2000). In this study, flotation was chosen as the method of floc separation. Successive stages in the selective flocculation process are illustrated in Figure 6.

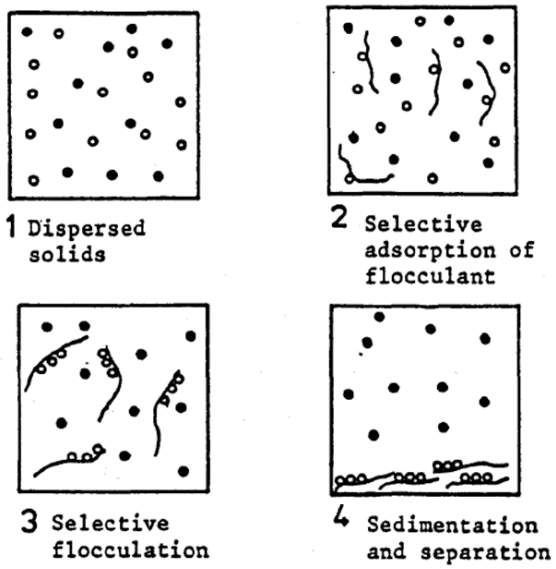

Figure 6 Stages of selective flocculation process. Modified from PhD dissertation by L.Spencer (1984).

The principles of selective flocculation as well as the underlying surface chemistry have been reviewed earlier by many authors (Attia, 1987; Attia & Fuerstenau, 1978; Attia & Kitchener, 1975; Attia, 1977; Friend & Kitchener, 1973; Moudgil et al., 1993; Somasundaran, 1980; Sresty et al., 1978; Yarar & Kitchener, 1970; Yu & Attia, 1987).

This research aims to study how different operating parameters influence flotation performance in the presence of a flocculant.

2.4.1 Flocculant

In selective flocculation, particle agglomeration is induced by adding a polymeric material (flocculant) in a dispersed phase (Mathur et al., 2000). Flocculants can be synthetic or natural polymers (Mathur et al., 2000; Somasundaran et al., 1996).

The effectiveness of flocculants can be determined by their ionic strength (negative or positive), molecular weight (or chain length), pH, the charge density of the molecule, backbone structure of the molecule (branched or linear), and the dosage of the flocculant (Rinne et al., 2023). In the study by Rinne et al., (2023), cationic flocculants were employed to selectively flocculate LCO from black mass, resulting in a high-quality graphite concentrate through selective flocculation.

2.5 Investigated Parameters in Flotation Optimization

Selectivity in flocculation operations is influenced by particle characteristics (e.g., particle size, particle surface heterogeneity, and surface potential), the electrochemical environment of the suspension (e.g., pH and other dissolved species), the properties of the flocculant polymers (e.g., ionic character and molecular weight), and the mechanical parameters of mixing (e.g., agitation rate and the type of impeller) (Rinne et al., 2023; Somasundaran et al., 1996; Somasundaran & Runkana, 2000).

Mechanical flotation machines are the most widely used equipment for ore beneficiation (Wang & Liu, 2021). Within a mechanical flotation cell, fluid turbulence levels and flow patterns are primarily determined by agitation intensity. Typically, the intensity of agitation is described by impeller tip speed which is the velocity at the far end of the rotor blades (Wang & Liu, 2021).

A high agitation rate has been shown to improve bubble-particle collision and thus the flotation rate of fine particles (Deglon, 2005; Jordan & Spears, 1990; Schubert, 1999; Tabosa et al., 2016). In fine particle flocculation flotation, intense agitation is required to provide sufficient kinetic energy for particles to overcome the energy barrier and aggregate. However, the intensity of agitation must be properly controlled, as it affects both the structure of the flocs and the flotation performance (Ding & Laskowski, 2007). Excessive mechanical stress can lead to floc breakdown, therefore determining the optimal agitation rate is crucial to promote effective floc formation and growth, facilitate bubble-particle attachment, and minimize the risk of floc breakage caused by mechanical forces (Šulc & Ditl, 2012). Under intense agitation, maintaining separation efficiency requires increased flocculant dosage. However, flocculation agents are costly, and overdosing can result in overly aggressive aggregation, which reduces selectivity (Šulc & Ditl, 2012). Therefore, dosage control is another critical parameter.

Under the shear turbulence of flotation, the aggregation of hydrophobic particles is a natural process driven by hydrophobic forces. Still it is not the only influencing factor that can improve their flotation recovery of hydrophobic particles (Wang & Liu, 2024). Polymer flocculation is a well-recognized operation that is broadly used in mineral processing industries, with plenty of scholarly articles (Ng et al., 2018; Oliveira & Rubio, 2012; Wang et al., 2011). It has been used in the flotation process for treating fine particles (Forbes, 2011; Yang & Song, 2014).

Rinne et al. (2023) suggested that controlling particle size via selective flocculation prevents cathode entrainment in black mass flotation. They suggested that branched cationic polyacrylamide (CatPAM) flocculants offer

promising results for graphite separation, indicating their potential for further research.

Ding and Laskowski, (2007) reported that flocculation of ash by a low-anionic polyacrylamide improved the cationic flotation recovery of ash and the separation efficiency, provided that a certain degree of shear was used (such as in a mechanical flotation cell). This moderate shear helps break heteroflocs and enhance selectivity.

Murhula et al., (2023) investigated the effects of particle size and solid concentration on flotation kinetics and entrainment in quartz and hematite single-mineral flotation systems. Their findings indicated that extending flotation time results in increased water recovery in the froth, which accelerates as mineral recovery approaches equilibrium. In the context of reverse flotation of iron ore, avoiding equilibrium recovery can help reduce entrainment, although this approach may not be applicable to direct flotation (Murhula et al., 2023). Additionally, their study found that higher flotation recovery of hematite is achieved at lower solid concentrations (Murhula et al., 2023).

These studies suggest that the flocculation process of black mass is a complex phenomenon, that requires studying the behaviors of multiple variables. This study will closely examine how various operating parameters, including solid content, impeller tip speed, conditioning time, and flocculant dosage, affect the system.

2.6 Design of Experiments (DOE)

According to Wu and Hamada (2009), design of experiment can be viewed as:

> *a body of knowledge and techniques that enables an investigator to conduct better experiments, analyze data efficiently, and make the connection between the conclusion from the analysis and the original objective of the investigation.*

Design of experiment (DOE) is a fundamental tool in engineering. This technique can be used mainly to improve the efficiency of processes. The basic idea of DOE is to systematically vary all relevant parameters across a range of conditions through a series of planned experiments, and then integrate the results using a mathematical model (Witek-Krowiak et al., 2014). Afterwards, this model can be gradually used for optimisation, predictions or interpretation allowing for improved process performance, reducing the number of variables in the process by considering only the most significant factors, and reducing operation costs and experimental time (Montgomery, 2010).

2.6.1 Response Surface Methodology

Response surface methodology (RSM) is a set of mathematical techniques that describe the relation between several independent variables and one or more responses (Witek-Krowiak et al., 2014). This method was developed by Box and Wilson (1951), and since then it has been widely used as an effective optimization technique for designing experiments in chemical processes (Abbaker & Aslan, 2023; Arroug et al., 2024; Taşdemir & Taşdemir, 2023; J. Wang et al., 2023).

The RSM method is based on the fit of mathematical models, linear, square polynomial functions and others to the experimental results generated from the designed experiment and the verification of the model obtained utilizing statistical techniques (Witek-Krowiak et al., 2014). The eventual objective of RSM, as mentioned by Myers and Montgomery (2016) is:

To determine the optimum operating conditions for the system or to determine a region of the factor space in which operating requirements are satisfied.

Several design strategies have been applied for RSM. The most popular methods are Central Composite Design (CCD), Box-Behnken Design (BBD), Doehlert matrix, Plackett-Burman Design, and Full or Fractional Factorial Design (FFD) (Ye et al., 2020). The basic model design strategies used in RSM are presented in Figure 7.

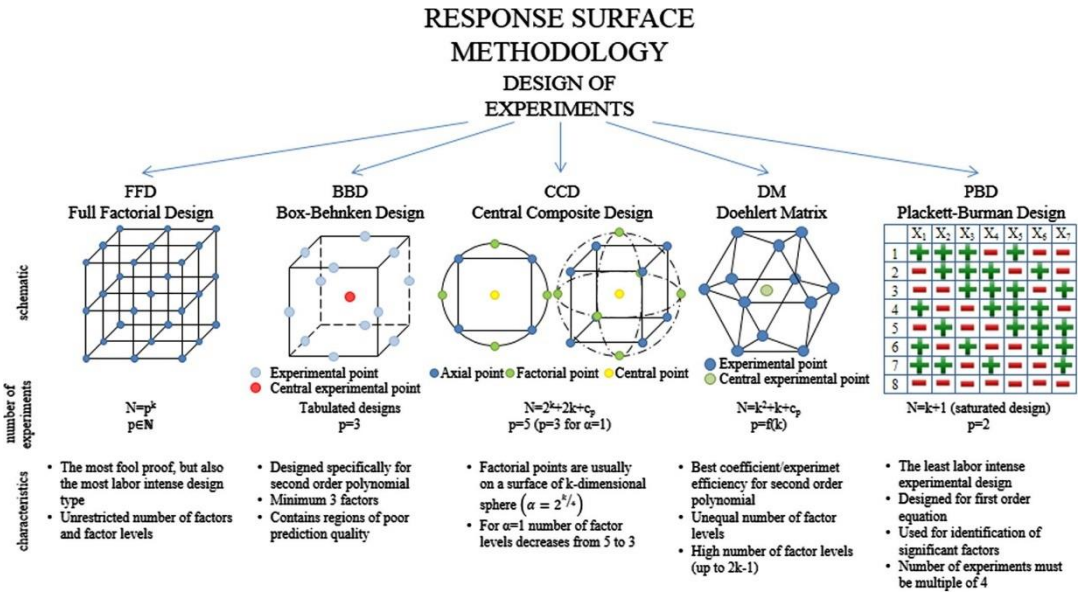

Figure 7 Basic model designs used in RSM (Witek-Krowiak et al., 2014).

2.6.2 Box-Behnken Design

The Box-Behnken design (BBD) was proposed by Box and Behnken (Box & Behnken, 1960), who developed the three-stage incomplete factorial design in 1960 as an alternative to the labour-intensive full factorial design (Arroug et al., 2024).

According to the experimental objectives outlined by the National Institute of Standard and Technology (NIST), the approach of this study aligns with RSM. The appropriate experimental designs for 2 to 4 factors are the CCD or BBD, as shown in Table 1.

Table 1 Design selection guideline (NIST).

Number of Factors	Comparative Objective	Screening Objective	Response Surface Method Objective
1	1-factor completely randomised design	-	-
2-4	Randomised block design	Full or fractional factorial	Central composite or Box-Behnken
5 or more	Randomised block design	Fractional factorial or Plackett-Burman	Screen first to reduce the number of factors

According to NIST, the Box-Behnken design is an independent quadratic design that does not contain an embedded factorial or fractional factorial design. In this design, the treatment combinations are at the midpoints of the edges of the process space and the centre. These designs are rotatable (or near rotatable) and require three levels of each factor. Figure 8 illustrates a Box-Behnken design for three factors.

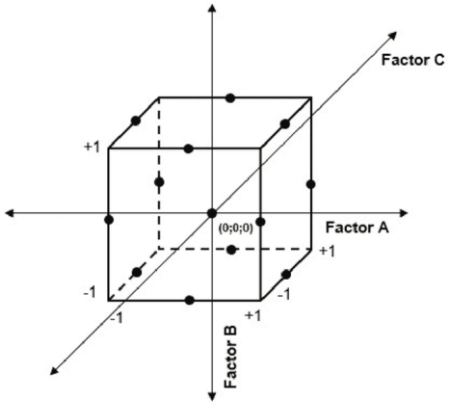

Figure 8 Geometric view of a three-factor Box-Behnken design (Peixoto et al., 2018)

The selective flocculation experiments aim to identify the optimal process conditions for four factors within a specified range, enabling a comparison with baseline experiments conducted without flocculant.

A review of research articles on the modelling and optimization of the flotation systems confirmed that, among various design methods employed, CCD and BBD are the most widely used for optimizing flotation. A summary of the reviewed articles is presented in Table 2.

Table 2 Optimization of flotation using RSM.

System	Feed	Method	Response	Reference
Selective Flotation	Phosphate ore	CCD	Grade, Recovery	(Derhy et al., 2024)
Cationic Flotation	Iron ore	CCD	%SiO2 conc., %Fe conc.	(Pinheiro et al., 2024)
Flotation	Polycarbonate (PC)	BBD	Grade, Recovery	(Witek-Krowiak et al., 2014)
Floc-Flotation	Wastewater	CCD	Recovery	(Taşdemir & Taşdemir, 2023)
Flotation	Coal	BBD	Recovery, Separation Efficiency	(Mohanty & Honakeri, 1999)
Flotation	Phosphate ore	D-Optimal Design	Grade, Recovery, Flotation rate constant	(Hoang et al., 2019)
Flotation	-	CCD	Flotation rate constant	(Hassanzadeh et al., 2019)
Flotation	Coal	CCD	Yield, ash level	(Kalyani et al., 2005)
Flotation	Coal	Fractional Factorial Design	Recovery, Pulp viscosity	(Dashti & Eskandari Nasab, 2013)
Flotation	Quartz particles	BBD	Recovery	(Abbaker & Aslan, 2023)
Reverse Flotation	Phosphate sludge	BBD	Grade, Recovery	(Arroug et al., 2024)
Flotation	Coal	BBD	Ash content, Flotation perfect index	(Ye et al., 2020)

Compared with central composite design and full-factorial design, BBD is more efficient in experimental design (Witek-Krowiak et al., 2014).

BBD was chosen for this study to identify the optimal set of variables, including solid content, impeller tip speed, conditioning time, and flocculant

dosage, and their main effects on the response variable, specifically graphite grade and recovery. This design is preferable when avoiding extreme conditions (too low or too high values) is important. Additionally, BBD requires fewer experimental runs to explore optimal conditions compared to the central composite design.

The statistical Software Minitab 10.0 was employed for data analysis and model building.

2.6.3 Statistical Analysis and Model Fitting

Analysis of Variance (ANOVA) is a versatile and powerful statistical technique used to analyze the difference between the means of more than two groups. The key outputs of ANOVA include the p-value and R^2 (Arroug et al., 2024). The p-value helps determine whether the differences between group means are statistically significant, while R^2 indicates how well the model fits the data (*Minitab, LLC*, 2021).

To determine if any of the differences between the means are statistically significant, the p-value is compared to the chosen significance level to assess the null hypothesis. The null hypothesis states that all population means are equal. Typically, a significance level (α) of 0.05 is used, indicating a 5% risk of concluding that a difference exists when there is no actual difference (*Minitab, LLC*, 2021).

The null hypothesis is rejected if the p-value is less than or equal to the significance level, indicating that not all population means are equal. If the p-value is greater than the significance level, there is insufficient evidence to reject the null hypothesis that the population means are all equal. Verifying that the test has enough power to detect a significant difference is essential (*Minitab, LLC*, 2021).

Following the execution of experiments, the responses were inputted into Minitab statistical software. Using the Box-Behnken design, optimal conditions for maximizing responses, graphite recovery, and grade were estimated by a quadratic model correlating variables with responses. Assuming that all variables are measurable, the general response form can be expressed as Equation 2 (Arroug et al., 2024):

$$Y = \beta + \beta_1 A + \beta_2 B + \beta_3 C + \beta_4 D + \beta_{12} AB + \beta_{13} AC + \beta_{14} AD + \beta_{23} BC + \beta_{24} BD + \beta_{34} CD + \beta_{11} A^2 + \beta_{22} B^2 + \beta_{33} C^2 + \beta_{44} D^2 \quad (2)$$

Where Y is the predicted response, β_i are constant coefficients, and A, B, C, and D represent the variables: solid content (g/L), flocculant conditioning time (min), impeller tip speed (rpm), and flocculant dosage (g/ton), respectively.

To determine how well the model fits the data, examine the goodness-of-fit statistics provided in the Model Summary table is Section 4.3.1, including R^2. R^2 represents the percentage of variation in the response that is explained by the model. The higher the R^2 value, the better the model fits the data. R^2 is always between 0% and 100% (*Minitab, LLC*, 2021).

2.7 Process Analysis and Evaluation Tools

2.7.1 Zeta Potential

Zeta potential (ZP) measures the effective electric charge on a nanoparticle's surface, quantifying its electrical characteristics. As illustrated in Figure 9, zeta potential is the electrokinetic potential measured at the slipping plane of the electric double layer. A shift of the slipping plane toward the bulk solution results in a smaller zeta potential (Matusiak & Grządka, 2017).

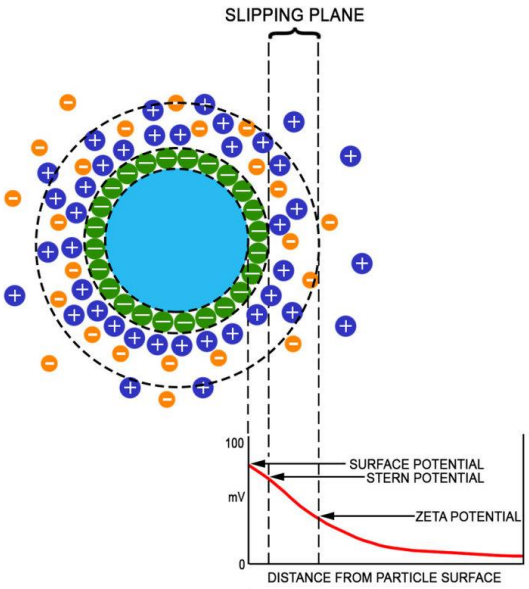

Figure 9 Schematic view of the electrical double layer (Matusiak & Grządka, 2017)

When a nanoparticle has a net surface charge, it is partially neutralized by a layer of ions of opposite charge located near the nanoparticle surface (Selvamani, 2019). This layer of oppositely charged ions moves with the nanoparticle, forming the electrical double layer. ZP measures the difference in potential between the bulk fluid in which a particle is dispersed and the layer of fluid containing the oppositely charged ions associated with the nanoparticle surface (Matusiak & Grządka, 2017). Particles with a positive zeta potential will bind to negatively charged surfaces and vice versa.

The magnitude of the zeta potential provides information about particle stability. The higher the magnitude of potential exhibits increased electrostatic

repulsion and therefore increased stability. It is important to consider that the zeta potential is influenced by the pH of the solution (Selvamani, 2019).

Understanding the zeta potential of both LCO and graphite at various pH levels is crucial for this study. First, these measurements clarify assumptions about how polymers adsorb onto the surfaces of LCO and graphite and provide insights into changes in surface potential. Second, these measurements help us identify the optimal pH for selectively adsorbing flocculants, given that pH is controlled consistently throughout the experiments.

ZP is measured by adding a solution to a cell that contains two electrodes. When a voltage is applied to the electrode, the particles will move toward the electrode with the opposite charge. A schematic representation of the zeta potential measurement is illustrated in Figure 10. The results of the zeta potential measurements are presented in Section 4.1.

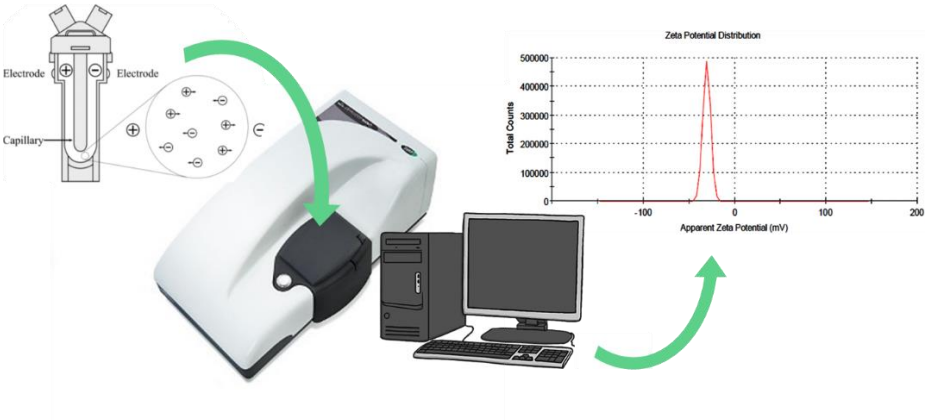

Figure 10 Schematic representation of the zeta potential measurements in a disposable folded capillary cell.

2.7.2 Particle Size Distribution

Particle size significantly impacts flotation performance. Fine particles often exhibit slow recovery rates due to their inertia and viscous drag, which reduces the frequency of particle-bubble collisions. They are also prone to entrainment and may experience excessive reagent adsorption due to their large specific surface areas and chemical reactivity. On the other hand, coarse particles, often face longer induction times and floatability deterioration, due to reduced adhesion forces and lower liberation (Feng & Aldrich, 1999; Fornasiero & Filippov, 2017).

In mineral processing, particles are categorized based on their size: fine to ultrafine particles are smaller than 20 µm; intermediate particles range from 20 to 250 µm; and coarse particles are larger than 250 µm .

2.7.3 Grade-Recovery Curves

The efficiency of metallurgical processes is commonly described using two terms: recovery and grade. Mineral separation via flotation can never achieve a 100% efficiency. This limitation is shown in a process-specific grade-recovery curve, as illustrated in Figure 11.

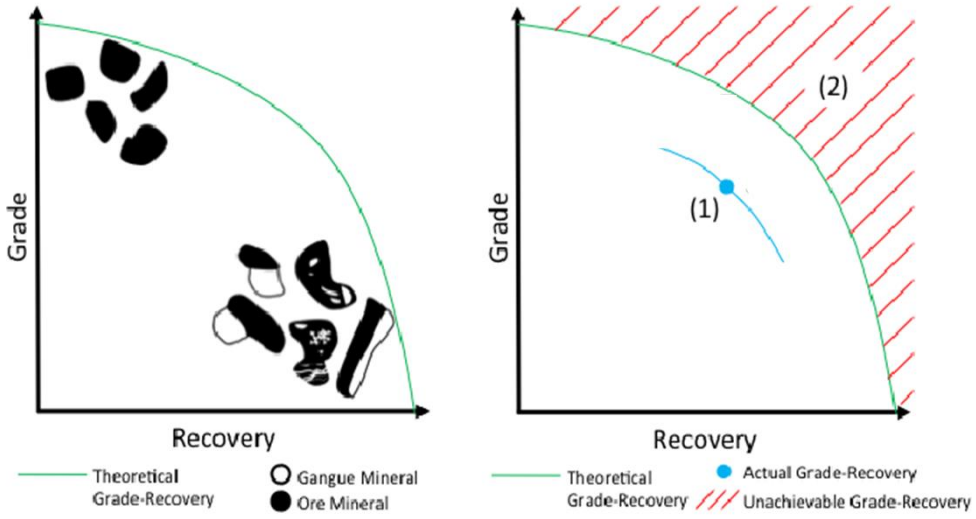

Figure 11 A schematic of the theoretical grade recovery curve (Bradshaw, 2014)

Figure 11 indicates that it is impossible to achieve both 100% grade and 100% recovery of the valuable mineral (Finch & Gomez, 1989). This limitation is due to the non-selective nature of entrainment and entrapment in a flotation system (Wills & Finch, 2015). The theoretical grade-recovery curve depends on particle liberation and the size distribution of the minerals (Stewart, 2010).

The green curve in Figure 11 represents the optimal grade-recovery performance of a flotation system. However, under non-optimal conditions, the grade-recovery will not follow this curve. The actual grade-recovery curve always lags behind the theoretical one due to varying particle sizes, imperfect liberation, and varying chemical composition (Spek & O'Keefe, 2014). The flotation process should always be optimized to find the best possible solution for balancing the grade-recovery trade-off (Wills & Finch, 2015).

2.7.4 Response Graph Analysis

The graphical tools are essential in visualizing and interpreting the relationship between variables and responses. These tools provide valuable insights into how input variables influence the outcomes of experiments. The following graphs are used in this study (*Minitab, LLC*, 2021):

- Pareto Chart: To compare the relative magnitude and statistical significance of main, square, and interaction effects in the experimental model. The chart displays the absolute values of the standardized effects, arranged in descending order. Minitab automatically plots these effects and includes a reference line indicating significant effects based on a default significance level of 0.05.
- Surface Plot: To plot the relationship between a fitted response and two continuous variables using a three-dimensional response surface plot, where the x- and y-axes denote the variables, and the response variable (z) is represented by a smooth surface.
- Contour Plot: To visualize the relationship between a fitted response and two continuous variables. This plot provides a two-dimensional representation where points sharing the same response value are connected by contour lines, allowing for a clear visualization of how the response varies across the range of the two variables.

The response graphs are presented in Chapter 4.

3 Research Material and Methods

3.1 Mineral Samples and Chemicals

3.1.1 Minerals

In this study, a synthetic black mass was prepared to simulate the composition of Li-ion battery waste. The synthetic black mass consisted of a mixture of LCO and graphite in a 1:1 wt.% ratio. This model black mass served as the primary material for the experimental campaign. The properties of the minerals are listed in Table 3.

Table 3 Properties of the minerals.

Mineral	Purity [%]	Particle Size [µm]	Distributor
$LiCoO_2$	>99.5	5-7	MSE Supplies, Tucson, AZ, USA
Spherodized Graphite	99.95	23	ProGraphite GmbH, Untergriesbach, Germany

3.1.2 Flocculant

Branched flocculants offer better selectivity than linear flocculants (Rinne et al., 2023). Results suggest that a concentration of 20 g/t is optimal for the selectivity of the flocculation process with FO 4498 (Rinne et al., 2023). Therefore, FO 4498 and AN 934 were utilized for this experiment campaign. The properties of these flocculants are reported in Table 4.

Table 4 Properties of the flocculant.

Trade Name	Ionicity	Polymer Backbone Structure	Abbreviation	Distributor
FO 4498 SSH	Medium cationic	Branched	FO 4498	SNF Floerger Andrézieux, France
AN 934 SH	Medium anionic	-	AN 934	SNF Floerger Andrézieux, France

Flocculant solutions were prepared 24 hours before the flotation tests and stirred overnight using a magnetic stirrer to ensure proper dissolution. The flocculant solution was prepared at a concentration of 0.5 wt.% by initially wetting the dry flocculant powder with ethanol at a 1:2 weight ratio and then adding deionized water using Elga Option-R 15BP water purification system (Veolia water, France) to reach the target concentration (Rinne et al., 2023). This solution was further diluted to 0.02 wt.% before the experiments. The

solution was used within 48 hours and discarded afterwards to ensure degraded flocculants were not used, as the age of the flocculant solution has been reported to influence its performance (Owen et al., 2002).

3.1.3 Flotation Reagents

The pH of the slurry was adjusted using hydrochloric acid (HCl) and sodium hydroxide (NaOH), both of which were of high purity (0.1 M, 99.5% purity). Additionally, methyl isobutyl carbinol (MIBC, 98% purity) was used as a frother to facilitate the froth flotation process (Rinne et al., 2023). All the chemicals were purchased from Sigma-Aldrich and were used without further purification.

3.2 Experimental Procedure

The experimental procedure was structured into several key stages to optimize the separation of graphite from Li-ion battery waste using froth flotation and selective flocculation methods. Initially, preliminary measurements such as zeta potential were conducted to determine the optimal pH condition for the pulp, followed by particle size distribution measurement to understand how the flocculant interacted with solid particles within the model black mass.

Experiments were designed using Minitab software to examine the interaction among studied variables in terms of grade and recovery. Laboratory experiments were subsequently executed under controlled conditions, where flocculants and flotation reagents were applied to assess their effectiveness in separating LCO and graphite.

The resulting flotation samples were analyzed using X-Ray Fluorescence (XRF) to quantify the concentrations of LCO and graphite in both the froth and tailings. Finally, data collected were analyzed using statistical methods in Minitab to interpret results and optimize conditions for maximizing graphite grade.

3.3 Zeta Potential Measurement

ZP Measurements were carried out using a Malvern Panalytical Zetasizer Nano ZS 90 (Malvern, United Kingdom). ZP values were measured in aqueous media within a pH range of 2–11. HCl and NaOH (0.1 M) were used to adjust the pH, and the pH was measured using a Mettler Toledo SevenExcellence™ multi-channel pH meter (Greifensee, Switzerland).

All graphite samples were ground for 60 s in a ring mill (Fritsch Pulverisette 9, Idar-Oberstein, Germany) with a tungsten carbide grinding media to

ensure the stability of dispersions during the measurements. LCO and ground graphite samples were dispersed in the pH-adjusted water to form 0.01 wt.% dispersions. Before each measurement, the dispersed samples were shaken vigorously for 30 s before pipetting them into a disposable folded capillary cell (cell type DTS1070). Based on the results of the ZP measurements, an optimal pH for selective flocculation was determined (Rinne et al., 2023).

3.4 Particle Size Distribution Measurement

Particle size distribution (PSD) of mineral dispersions of LCO and graphite were measured at various flocculant dosages to investigate the interaction between flocculants and solid particles. PSDs were measured using a laser diffraction particle size analyzer (Malvern Panalytical Mastersizer 3000, Malvern, United Kingdom).

The measurements were conducted in an aqueous medium at pH 5.6, which was determined to be the most suitable pH for selective flocculant adsorption based on zeta potential measurements (discussed in Section 4.2).

Each PSD sample was prepared as follows (Rinne et al., 2023):

1. A mineral sample was dispersed into 25 mL of water, adjusted to pH 5.6 using HCl, and shaken vigorously by hand for 2 minutes to ensure proper mixing.
2. The desired amount of flocculant was added to the dispersion and shaken vigorously by hand for 3 minutes to promote floc formation and growth.
3. The sample was then added to 500 mL of pH 5.6-adjusted water, and the measurement was initiated immediately.

Five measurements were carried out for each sample, and an average distribution was calculated.

3.5 Flotation Using DOE

The four independent operational variables considered for the study were solid content (g/L), flocculation conditioning time (min), impeller tip speed (rpm), and flocculant dosage (g/ton). The first three factors are continuous variables, while the flocculant dosage is a categorical variable. Continuous variables are numeric variables that have an infinite number of values between any two values, however, categorical variables contain a finite number of categories or distinct groups. The levels of the variables studied are

presented in Table 5. Graphite recovery and grade were measured as response variables.

Table 5 Operational variables and their levels.

	Code	Factor's Name	Level 1	Level 2	Level 3
Continues factors	**A**	Solid content (g/L)	20	40	60
	B	Flocculant conditioning time (min)	2	6	10
	C	Impeller tip speed (rpm)	900	1300	1700
Categorial factor	**D**	Flocculant dosage (g/ton)	20	-	50

The parameter levels are denoted with specific colors: yellow for the minimum level (level 1), green for the mid-level (level 2), and red for the maximum level (level 3).

Box-Behnken design was employed to design the experiments using Minitab software. The DoE obtained consisted of 26 experimental runs, thoroughly exploring the impact of the four independent operational variables on graphite recovery and grade. Table 6 presents the detailed experimental setup for each of the 26 runs, specifying the solid content, flocculation conditioning time, flocculant dosage, and impeller tip speed levels used in each experiment.

Table 6 Experiment setup using Box-Behnken design.

Run	Solid content (g/L)	Flocculant conditioning time (min)	Impeller tip speed (rpm)	Flocculant dosage (g/ton)
1	20	2	1300	20
2	60	2	1300	20
3	20	10	1300	20
4	60	10	1300	20
5	20	6	900	20
6	60	6	900	20
7	20	6	1700	20
8	60	6	1700	20
9	40	2	900	20
10	40	10	900	20
11	40	2	1700	20
12	40	10	1700	20
13	40	6	1300	20
14	20	2	1300	50
15	60	2	1300	50
16	20	10	1300	50

17	60	10	1300	50
18	20	6	900	50
19	60	6	900	50
20	20	6	1700	50
21	60	6	1700	50
22	40	2	900	50
23	40	10	900	50
24	40	2	1700	50
25	40	10	1700	50
26	40	6	1300	50

Experiments were performed using a manually operated batch flotation machine (Outokumpu batch flotation machine), in a 1 L flotation cell. The flotation machine is shown in Figure 12.

Figure 12 Outokumpu batch flotation machine.

The model black mass was placed in the flotation cell, followed by the addition of 1 L of ion-exchanged water. The pulp was adjusted to pH 5.6 after the addition of the black mass using HCl, as measured with a Mettler Toledo SevenExcellence™ multi-channel pH meter (Greifensee, Switzerland), achieving the desired solid-liquid ratio. The pulp was then agitated with an impeller for 3 minutes to ensure proper mixing before adding surfactants. The flocculant was then added, and the mixture was stirred for an additional

time based on the flocculant conditioning time. Finally, the frother was added, with a conditioning time of 2 minutes, and the air was introduced at the bottom of the cell through an outlet in the impeller at a constant flow rate of 2 L/min. The pH of the pulp was continuously controlled throughout the experiments. Figure 13 provides a schematic representation of the experimental procedure, and the parameters kept constant during the experiments.

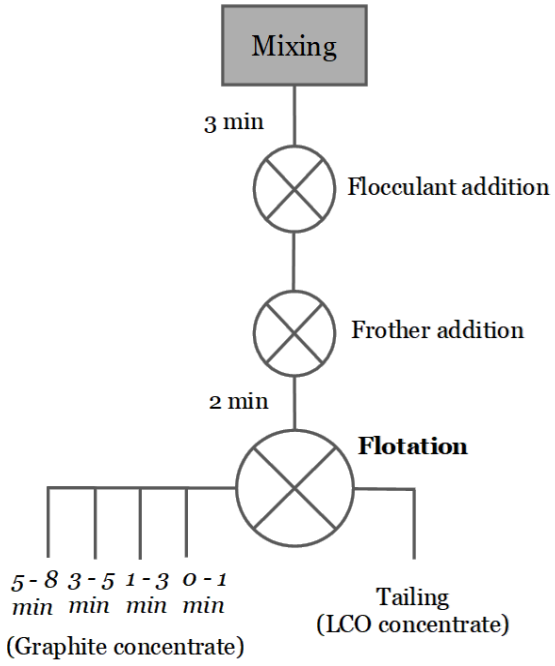

Figure 13 Schematic representation of the experimental procedure for flotation.

Once the airflow began, froth formation started, marking the beginning of the experiment ($t_{0\ min}$). The first froth concentrate fraction was collected during the first minute of the experiment ($t_{0-1\ min}$) by continuously scooping the froth into a container. The second froth concentrate was collected by scooping during the timeframe $t_{1-3\ min}$. The third and fourth froth concentrates were collected during the periods $t_{3-5\ min}$ and $t_{5-8\ min}$, respectively. The collected concentrates and underflow were then vacuum-filtered and air-dried in a convection oven (Ecocell, EC 404, MMM Medcenter Einrichtungen, Germany) at 40°C for approximately 48 hours. Figure 14 shows a froth fraction collected during the experiment.

Figure 14 Froth fraction.

3.5.1 Sample Characterization and Analysis

3.2.5.1 X-ray Fluorescence

Once the samples were dried, their mass fraction was measured using a laboratory scale (Precisa Instruments Ltd., XB 6200D, Switzerland). The samples were transferred from the filter papers into small plastic bags for elemental composition characterization. A portable X-ray fluorescence (XRF) gun (Oxford Instruments, X-MET 5100, Abingdon, United Kingdom) was used for this purpose, as shown in Figure 15.

The measurement mode was set to "Mining FP" with a duration of 60 seconds for each measurement. Three measurements were taken for each sample fraction to ensure accuracy, and the results were averaged. The XRF gun was pointed at different areas of the sample during each measurement to avoid biased information.

Figure 15 The portable X-ray fluorescence (XRF) gun.

As the XRF gun could only analyze elements with atomic numbers ≥ 20, Co was used as a marker element for cathode particles (Rinne et al., 2024). A calibration curve was obtained from mixtures of LCO and graphite with known compositions to improve the quantitative accuracy of the XRF analysis. To generate the calibration curve, data points were collected at 0.5 wt.% intervals for the LCO grade range of 0–5 wt.%, at 10 wt.% intervals for the LCO grade range of 10–90 wt.%, and at 0.2 wt.% intervals for the LCO grade range of 90–100 wt.%. The resulting curve was then used as a reference to adjust the measured XRF results and to transcribe the measured Co into LCO grades (Rinne et al., 2023; Rinne et al., 2024). The calibration curves are provided in Appendix A.

The composition of the underflow was calculated via a mass balance of the LCO content of the froth fractions and the known head grade of the flotation feed. In these calculations, the LCO and graphite head grades were adjusted based on the assumption that Li partially dissolves in the process water during flotation (Salces et al., 2022).

4 Results and Discussions

4.1 Zeta Potential Measurement

Figure 16 indicates the ZP values of graphite and LCO as a function of pH of the dispersed solution. HCl and NaOH were used as pH regulating agents, resulting in the dominant ions in the pulp being H^+ and Cl^- for the acidic pH range, and Na^+ and OH^- for the basic pH range (Rinne et al., 2023).

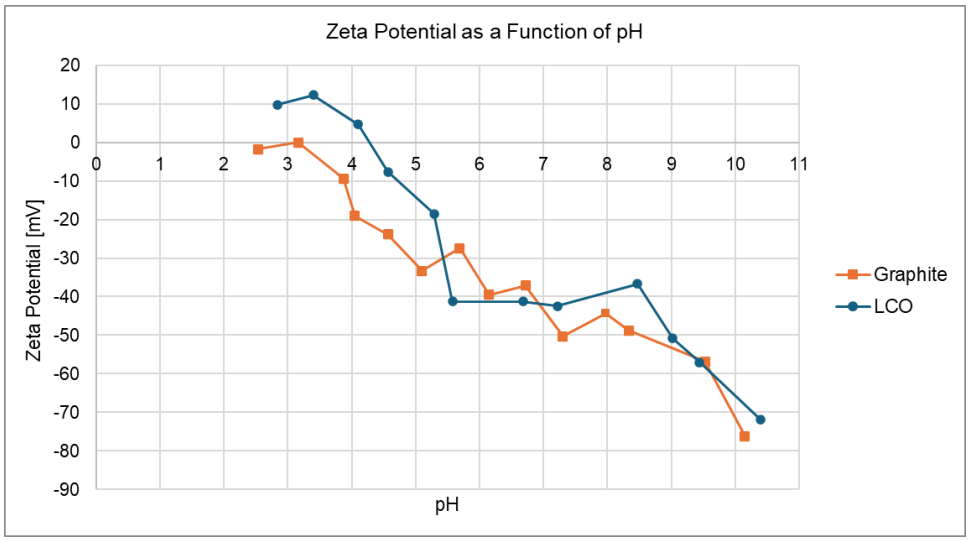

Figure 16 Zeta potential of graphite and LCO as a function of pH.

As shown in Figure 16, the ZP measurements indicate that under the studied pulp conditions, the surface charge of graphite is approximately neutral or slightly negative in the pH range of 2.5–4, becoming increasingly negative from pH 4 to 10. In contrast, LCO shows a slightly positive surface charge in the pH range of 3–4, transitioning to a highly negative charge between pH 5 and 10. The isoelectric point of LCO is between pH 4 and pH 5. Considering that neither LCO nor graphite contain chemically reactive functional groups, it is likely that the change in zeta potential at different pH levels results from the adsorption of ionic species of water (Rinne et al., 2023).

When identifying the candidate pH range for electrically selective flocculant adsorption on the LCO surface, a pH range of 3–4 would thus be favourable for anionic flocculants, and pH 5.6 for cationic flocculants as there is a difference in the surface charge of the two components in this region.

To minimize reagent consumption and avoid working in an aggressive system with pH 3, and considering scalability, pH 5.6 was selected for further study. At this pH, it is expected that a cationic flocculant will preferentially adsorb onto the highly negative LCO surface rather than the comparatively

less negatively charged graphite surfaces. This hypothesis was tested through particle size measurements of single active components with varying flocculant dosages (Rinne et al., 2023).

4.2 Particle Size Distribution

Particle size distributions were measured for pure LCO and graphite at pH 5.6 and pH 3.4 to study the effect of flocculant concentration on particle size. FO 4498 was used as the cationic flocculant at pH 5.6, while AN 934 was used as the anionic flocculant at pH 3.4. PSDs were initially measured for samples without any flocculants, and these were used as baselines for comparison with the PSDs of flocculated samples.

Figure 17 shows the frequency of PSDs of LCO samples as a function of flocculant concentration.

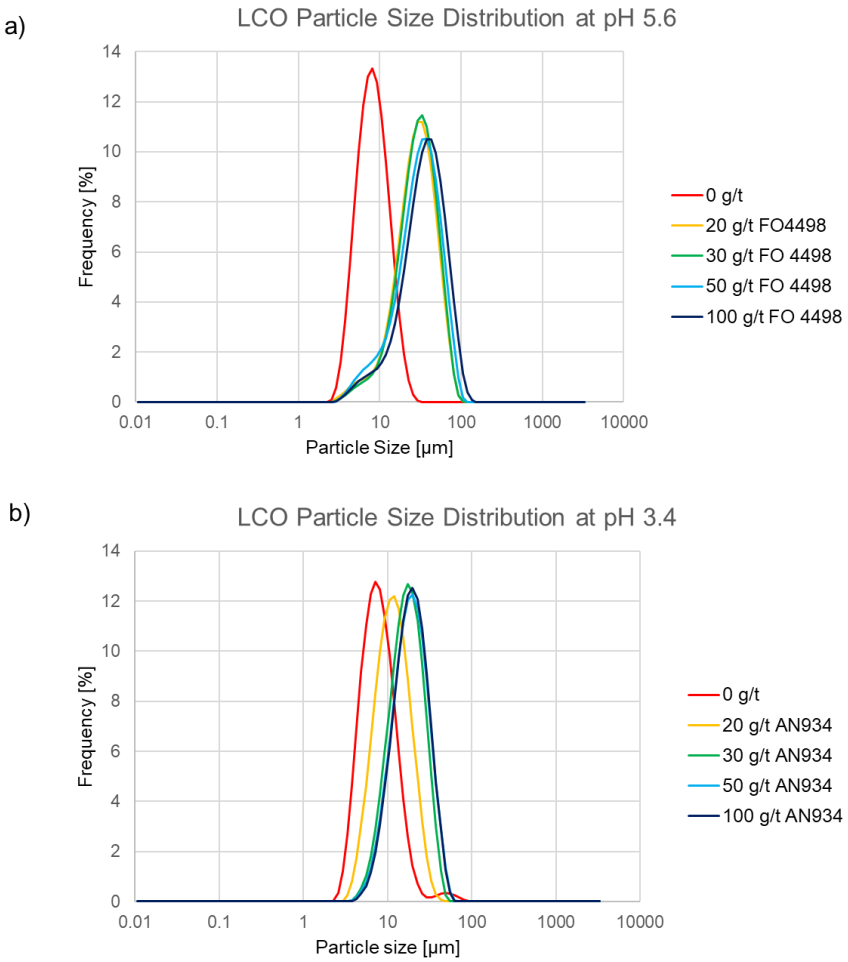

Figure 17 Particle size frequency distributions of LCO a) with varying concentrations of the cationic flocculant FO 4498 at pH 5.6, and b) different concentrations of the anionic flocculant AN 934 at pH 3.4.

As shown in Figure 17, LCO samples interact with both the cationic and anionic flocculant, resulting in a consistent increase in the particle size with higher flocculant concentration. Even a relatively small addition of 20 g/t significantly influenced particle size. PSDs at pH 5.6 indicate that larger particle sizes were achieved with the cationic flocculant compared to the anionic flocculant, further supporting our choice of pH 5.6 for this study.

At pH 5.6, it is observed that flocculant dosages of 20 g/t and 30 g/t exhibit similar behaviour, as do 50 g/t and 100 g/t of FO 4498. Therefore, 20 g/t and 50 g/t were selected as the optimal and excess flocculant dosages for the flocculation-flotation experiments.

Based on the data presented in Figure 11 (a), 20 g/ton is sufficient to achieve a noticeable change in the PSD, as the PSDs remain almost the same in the range of 20-100 g/ton. Furthermore, research conducted by Rinne et al., 2023, indicates that overdosing the flocculant results in a loss of selectivity. Therefore, to maintain effectiveness while minimizing concentration, 20 g/ton was selected.

Regarding the effect of flocculant on graphite, Figure 18 presents the PSDs of pristine graphite particles and those in the presence of 50 g/t of both the cationic and anionic flocculants.

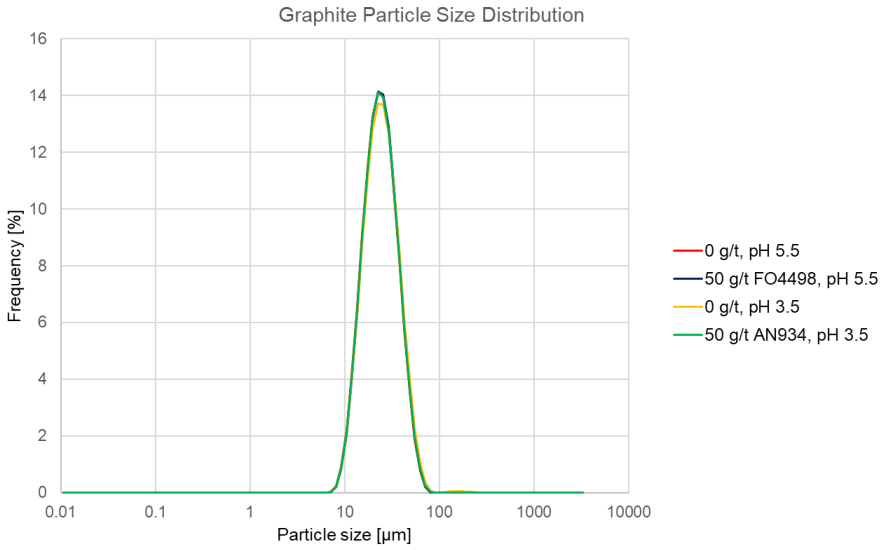

Figure 18 Particle size frequency distributions of graphite with both flocculants.

As shown in Figure 18, the particle size distribution of graphite is unaffected by both the cationic and anionic flocculants, even at a relatively high dosage of 50 g/t.

These results confirm that the studied flocculants do not adsorb onto the graphite surface, suggesting that the studied flocculants could potentially be used to agglomerate the LCO-graphite mixture selectively.

4.3 Floc-flotation Results

To explore the effect of the studied parameters presented in Table 7 on flotation performance (graphite recovery and grade), a Box-Behnken design was made. A total of 26 flotation tests were performed in a laboratory flotation cell. The BBD was generated using Minitab software, and the results of these experiments are shown in Table 7. The grade and recovery data listed in Table 10 represent the cumulative grade and the cumulative recovery of graphite over the 0-8 min flotation time.

Table 7 Box–Behnken design and the results of experiments. (A: solid content [g/L], B: flocculant conditioning time [min], C: impeller tip speed [rpm], and D: flocculant dosage [g/t])

Run	Factor's code				Graphite (%)	
	A	B	C	D	Recovery	Grade
1	20	2	1300	20	72.28	97.66
2	60	2	1300	20	70.77	95.08
3	20	10	1300	20	71.98	98.63
4	60	10	1300	20	75.73	95.32
5	20	6	900	20	74.57	97.28
6	60	6	900	20	63.44	95.70
7	20	6	1700	20	71.78	98.11
8	60	6	1700	20	80.57	95.70
9	40	2	900	20	65.36	96.48
10	40	10	900	20	55.62	97.28
11	40	2	1700	20	84.41	93.85
12	40	10	1700	20	76.81	91.43
13	40	6	1300	20	78.80	94.07
14	20	2	1300	50	62.44	98.13
15	60	2	1300	50	48.50	95.41
16	20	10	1300	50	60.43	97.96

17	60	10	1300	50	51.42	95.39
18	20	6	900	50	39.71	96.13
19	60	6	900	50	40.19	86.44
20	20	6	1700	50	72.53	95.87
21	60	6	1700	50	57.15	93.91
22	40	2	900	50	55.91	93.71
23	40	10	900	50	39.28	94.35
24	40	2	1700	50	65.88	91.75
25	40	10	1700	50	60.43	93.89
26	40	6	1300	50	59.52	96.18

4.4 Grade-Recovery Curves

Some of the grade-recovery curves are shown in the following figures. As seen in Figure 19, with a constant solid content of 40 g/L and a constant impeller tip speed of 900 rpm, flocculant dosage has a more significant impact on the performance of the system compared to conditioning time. This behavior might be due to the fact that at lower solid concentrations, the flocculant's role in promoting effective flocculation and separation is more significant.

Figure 19 indicates that increasing the conditioning time from 2 min to 10 min improves the grade, which aligns with the fact that extended conditioning allows for better floc formation and interaction (Ding & Laskowski, 2007). Additionally, experiments with lower flocculant dosages show better performance, resulting in higher grade and recovery. This might be because excessive flocculant can lead to the formation of heteroflocs, which are less effective for separating graphite.

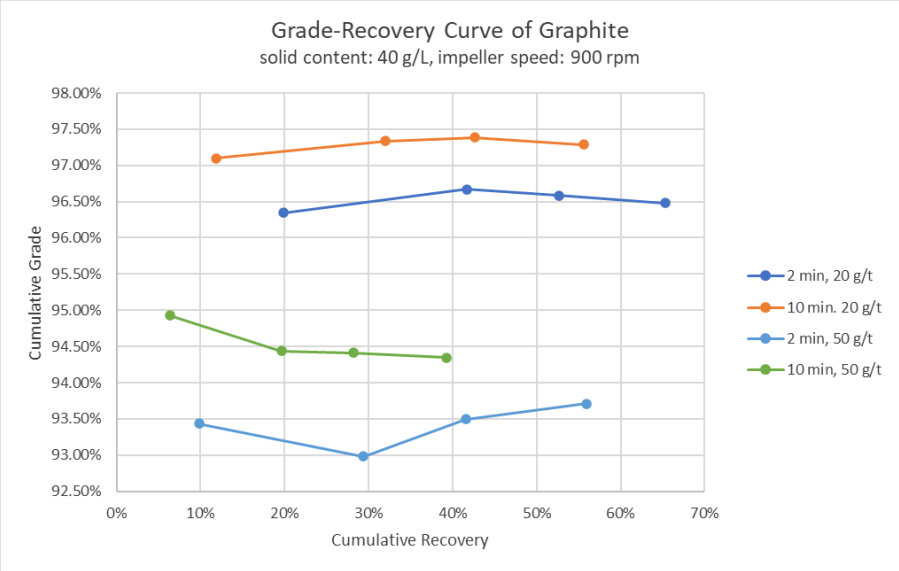

Figure 19 Grade-Recovery curve of graphite at a constant solid content of 40 g/L and a constant impeller tip speed of 900 rpm, showing the effects of varying conditioning times (min) and flocculant dosages (g/t) on performance.

At a high solid content of 60 g/L, the effect of varying conditioning time and flocculant dosage show minimal difference in grade, as shown in Figure 20. The reduction in performance at higher solid contents may be attributed to the increased complexity in managing flocculation and the potential for floc breakdown under high solid loadings.

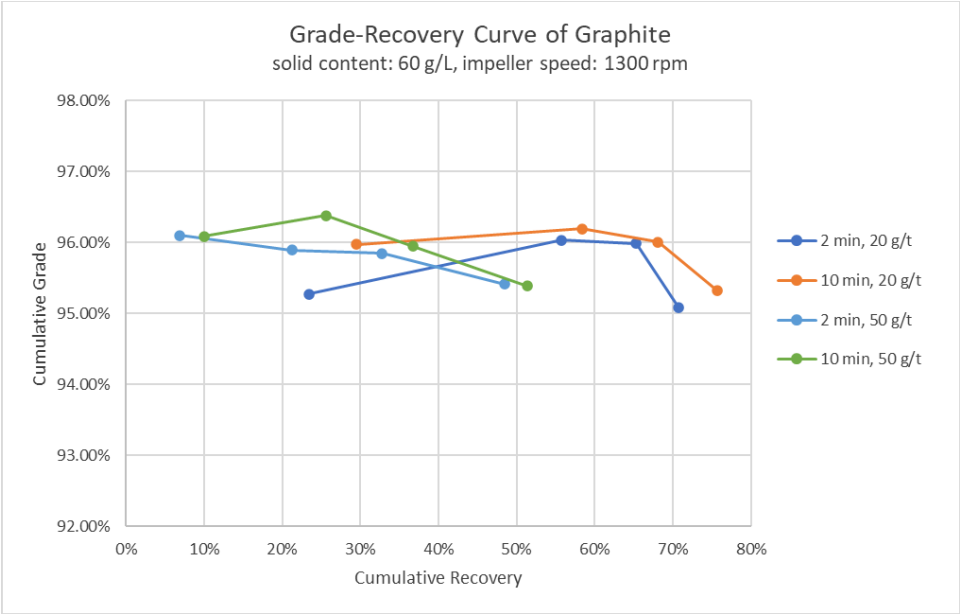

Figure 20 Grade-Recovery curve of graphite at a constant solid content of 60 g/L and a constant impeller tip speed of 1300 rpm, showing the effects of varying conditioning times (min) and flocculant dosages (g/t) on performance.

Further analysis in Figures 21 and 22 indicates that with constant conditioning time and impeller tip speed, solid content has a more significant impact on graphite grade compared to flocculant dosage. This observation supports findings that solid concentration significantly influences flotation efficiency and flocculation behavior (Murhula et al., 2023).

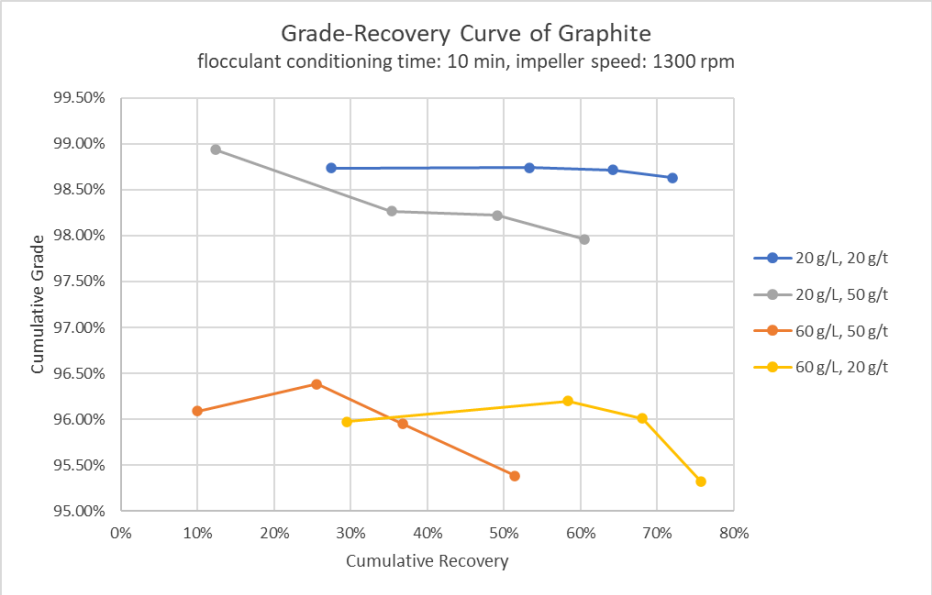

Figure 21 Grade-Recovery curve of graphite at a constant flocculant conditioning time of 10 min and a constant impeller tip speed of 1300 rpm, showing the effects of varying solid contents (g/L) and flocculant dosages (g/t) on performance.

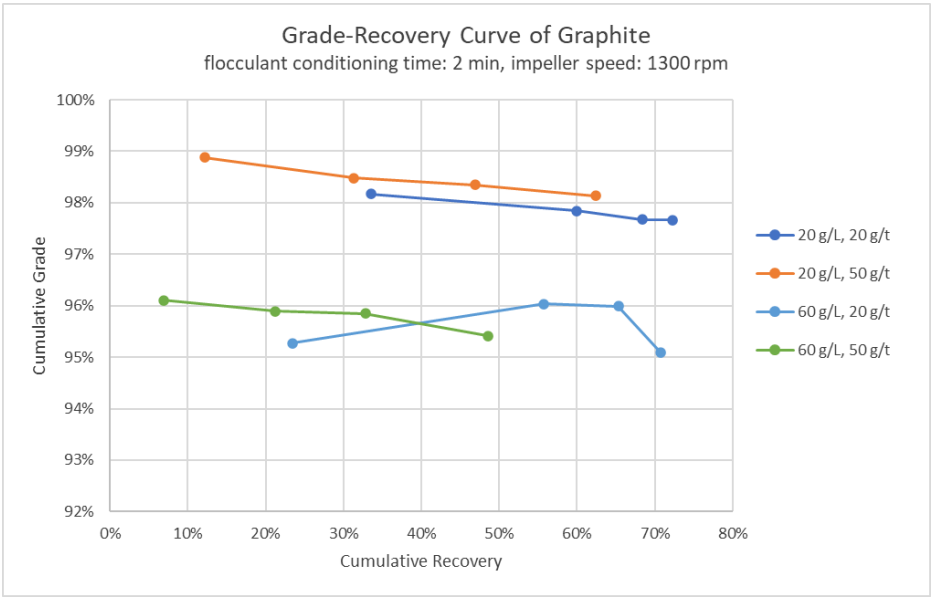

Figure 22 Grade-Recovery curve of graphite at a constant flocculant conditioning time of 2 min and a constant impeller tip speed of 1300 rpm, showing the effects of varying solid contents (g/L) and flocculant dosages (g/t) on performance.

The results suggest that while flocculant dosage and conditioning time are crucial at lower solid contents, their effects diminish at higher solid concentrations. The significance of the impact of these parameters will be further discussed in the following sections.

4.5 Response Surface Design Analysis

4.5.1 Regression Model Equations

According to the experimental results in Table 7, the response function of the second order representing graphite grade and recovery can be expressed as a function of the three continuous factors (A: solid content (g/L), B: flocculant conditioning time (min), C: impeller tip speed (rpm)). Minitab generates different regression models for each value of the categorial factor (D: flocculant dosage (g/t)). Equations (3) to (6) give the quadratic models that show the relationship between variables and responses:

For D=20 g/t:

$$Graphite\ grade = 0.964 - 0.00434\,A - 0.0009\,B + 0.000172\,C + 0.000030\,A * A + 0.000242\,B * B - 0.000000\,C * C - 0.000009\,A * B + 0.000001\,A * C - 0.000001\,B * C \quad (3)$$

For D=50 g/t:

$$Graphite\ grade = 0.912 - 0.00479\,A + 0.0000\,B + 0.000210\,C + 0.000030\,A * A + 0.000242\,B * B - 0.000000\,C * C - 0.000009\,A * B + 0.000001\,A * C - 0.000001\,B * C \quad (4)$$

For D=20 g/t:

$$Graphite\ recovery = 0.158 + 0.00365\,A - 0.0070\,B + 0.000724\,C - 0.000068\,A * A - 0.00141\,B * B - 0.000000\,C * C + 0.000159\,A * B + 0.000001\,A * C + 0.000010\,B * C \quad (5)$$

For D=50 g/t:

$$Graphite\ recovery = -0.015 + 0.00129\,A - 0.0096\,B + 0.000807\,C - 0.000068\,A * A - 0.00141\,B * B - 0.000000\,C * C + 0.000159\,A * B + 0.000001\,A * C + 0.000010\,B * C \quad (6)$$

To determine how well the model fits the data, the goodness-of-fit statistics should be considered which are provided in the Table 8.

Table 8 Model summary table.

	R-sq
Graphite grade	62.95%
Graphite recovery	88.54%

The higher the R^2 value, the better the model fits the data. Therefore, as presented in Table 8, the graphite recovery model fits the data better as the R^2 is 88.54%. The results of the experiments were subjected to analysis of variance (ANOVA) for both response variables, which will be discussed further in the following section.

4.5.2 Analysis of Variance

ANOVA is a statistical technique used to estimate the significance of the factors affecting a response variable by analyzing variance among different groups. The results of the ANOVA of the developed models are presented in Table 9.

Table 9 Variance calculation of regression model using Minitab. (A: solid content [g/L], B: flocculant conditioning time [min], C: impeller tip speed [rpm], and D: flocculant dosage [g/t])

Source	Variance calculation of the Graphite Grade regression model					Variance calculation of the Graphite Recovery regression model				
	Df	Sum of Squares	Mean of Squares	F-Value	P-Value	Df	Sum of Squares	Mean of Squares	F-Value	P-Value
Model	13	0.0106	0.0008	1.57	0.222	13	0.3572	0.0275	7.14	0.001
Linear	4	0.0058	0.0014	2.77	0.077	4	0.3321	0.0830	21.55	0.000
A	1	0.0045	0.0045	8.66	0.012	1	0.0090	0.0090	2.34	0.152
B	1	0.0000	0.0000	0.06	0.815	1	0.0072	0.0072	1.86	0.198
C	1	0.0001	0.0001	0.10	0.760	1	0.1147	0.1147	29.78	0.000
D	1	0.0012	0.0012	2.27	0.158	1	0.2012	0.2012	52.24	0.000
Square	3	0.0029	0.0010	1.84	0.194	3	0.0078	0.0026	0.67	0.586
A*A	1	0.0006	0.0006	1.25	0.286	1	0.0034	0.0034	0.88	0.367
B*B	1	0.0001	0.0001	0.13	0.722	1	0.0023	0.0023	0.60	0.453
C*C	1	0.0009	0.0009	1.77	0.208	1	0.0071	0.0071	1.85	0.199
2-Way Interaction	6	0.0020	0.0003	0.63	0.702	6	0.0174	0.0029	0.75	0.619
A*B	1	0.0000	0.0000	0.01	0.929	1	0.0013	0.0013	0.34	0.572
A*C	1	0.0006	0.0006	1.15	0.305	1	0.0002	0.0002	0.05	0.820
A*D	1	0.0003	0.0003	0.60	0.453	1	0.0089	0.0089	2.31	0.154
B*C	1	0.0000	0.0000	0.07	0.794	1	0.0022	0.0022	0.58	0.462
B*D	1	0.0001	0.0001	0.11	0.749	1	0.0004	0.0004	0.12	0.739
C*D	1	0.0010	0.0010	1.86	0.197	1	0.0043	0.0043	1.13	0.310
Error	12	0.0062	0.0005	*	*	12	0.0462	0.0039	*	*
Total	25	0.0168	*	*	*	25	0.4035	*	*	*

Variables with a p-value less than 0.05 play an important role in changing the responses, and the effect of variables with p-values greater than 0.05 is not significant. The F-value shows the importance degree and effectiveness of the variable (Ye et al., 2020). Minitab uses the F-value to calculate the p-value, which is used to determine the statistical significance of the test (*Minitab, LLC*, 2021).

According to Table 8, solid content has the most significant influence on the graphite grade, while impeller tip speed and flocculant dosage have the most impact on the recovery of graphite. This conclusion is based on the p-values for these factors, which are lower than 0.05, indicating statistical significance.

4.5.3 Pareto Charts

A Pareto chart is a particular type of bar chart where the plotted values are arranged from the largest to the smallest. The Pareto chart shows the absolute values of the standardized effects and plots a reference line to indicate which effects are statistically significant. On the Pareto chart, bars that cross the reference line are statistically significant. Figures 23 and 24 show the Pareto chart of the standardized effects of the parameters for grade and recovery.

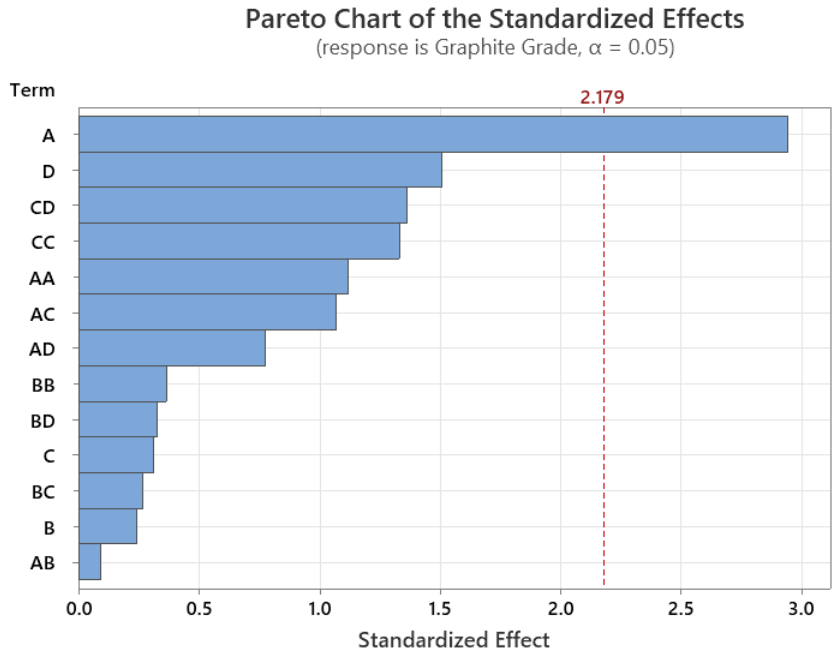

Figure 23 Pareto chart of standardized effects for the response variable: graphite grade. (A: solid content [g/L], B: flocculant conditioning time [min], C: impeller tip speed [rpm], and D: flocculant dosage [g/t])

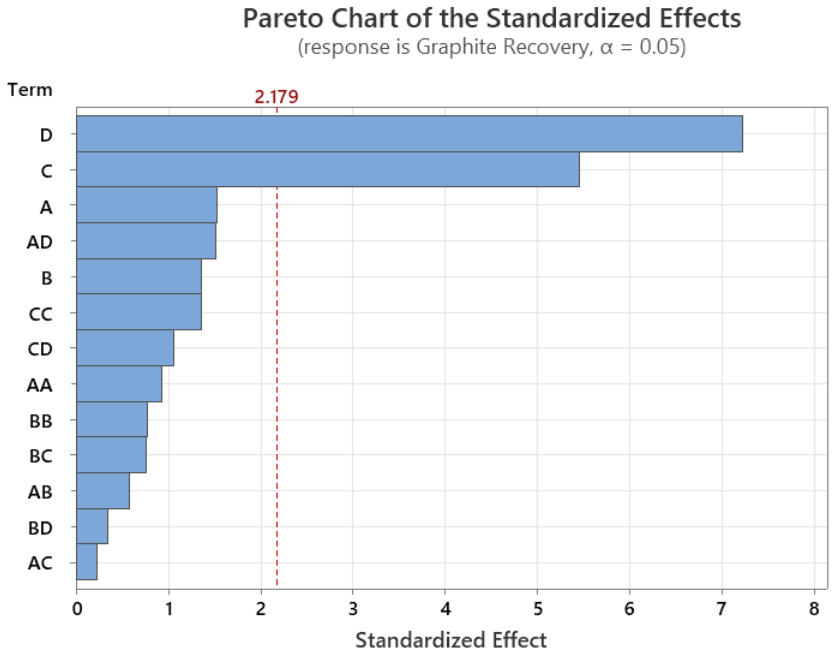

Figure 24 Pareto chart of standardized effects for the response variable: graphite recovery. (A: solid content [g/L], B: flocculant conditioning time [min], C: impeller tip speed [rpm], and D: flocculant dosage [g/t])

Figure 23 shows that coded factor A, representing solid content, has a statistically significant influence on the graphite grade. Figure 24 illustrates that factors C and D, which correspond to impeller tip speed and flocculant dosage, respectively, have a higher impact on graphite recovery.

Since the Pareto chart displays the absolute value of the effects, it can be used to determine which variables have a higher influence on the response, but it cannot be used to determine which effects increase or decrease the response (*Minitab, LLC*, 2021).

4.5.4 Surface Plots

Figure 25 represents the response surfaces that show the relationship between the graphite grade and the flotation process parameters to visualize better the effect of these variables on the flotation performance. In every surface plot, two factors were kept constant and listed as the hold value.

Figure 25 (a) represents the effect of solid content and flocculant conditioning time on the graphite grade. As shown in Figure 25 (a), a higher grade of graphite is obtained with a solid content of 20 g/L, and as it can be seen solid content plays a more critical role in affecting grade compared with flocculant conditioning time.

Figure 25 (b) shows the effect of solid content and impeller tip speed on the graphite grade. As can be seen, a higher grade is obtained at a medium-level

impeller tip speed and a lower solid content. When the solid content is kept constant, the grade increases with the increase of the impeller tip speed until a mid-level and decreases afterwards.

Figure 25 (c) shows the effect of flocculant conditioning time and impeller tip speed on graphite grade. According to Figure 25 (c), a low level of impeller tip speed is associated with a higher grade value.

It can be concluded that flocculant conditioning time has the minimal effect on the grade compared with other studied parameters. Also, a lower solid content tends to increase the grade significantly.

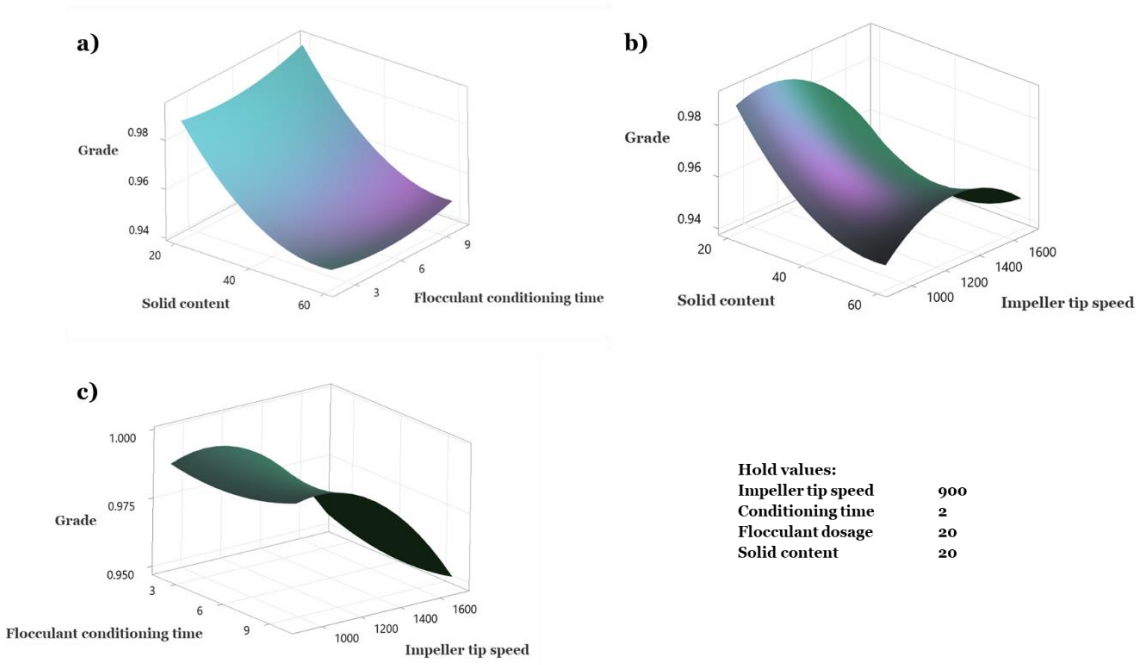

Figure 25 Response surface plots of grade. a) Effect of solid content (g/L) and flocculant conditioning time (min), b) Effect of solid content (g/L) and impeller tip speed (rpm), and c) Effect of flocculant conditioning time (min) and impeller tip speed (rpm).

The relationships between the flotation process parameter and graphite recovery are shown in Figure 26 as the response surfaces in a 3D plot. Figure 26 (a) represents the effect of solid content and flocculant conditioning time on graphite recovery. A higher recovery is obtained at a low level of solid content. In addition, when solid content is high, a better recovery is associated with a medium level of the flocculant conditioning time.

Figure 26 (b) shows the effect of solid content and impeller tip speed on the graphite recovery. Results indicate that recovery increased with the increase

of the impeller tip speed, which is due to the more significant number of particle-bubble collisions that happen at a high impeller tip speed at a constant airflow rate (Schubert & Bischofberger, 1978).

In addition, as shown in Figure 26 (c), which indicates the effect of flocculant conditioning time and impeller tip speed, impeller tip speed plays a significant role in graphite recovery. These results are compatible with those of ANOVA.

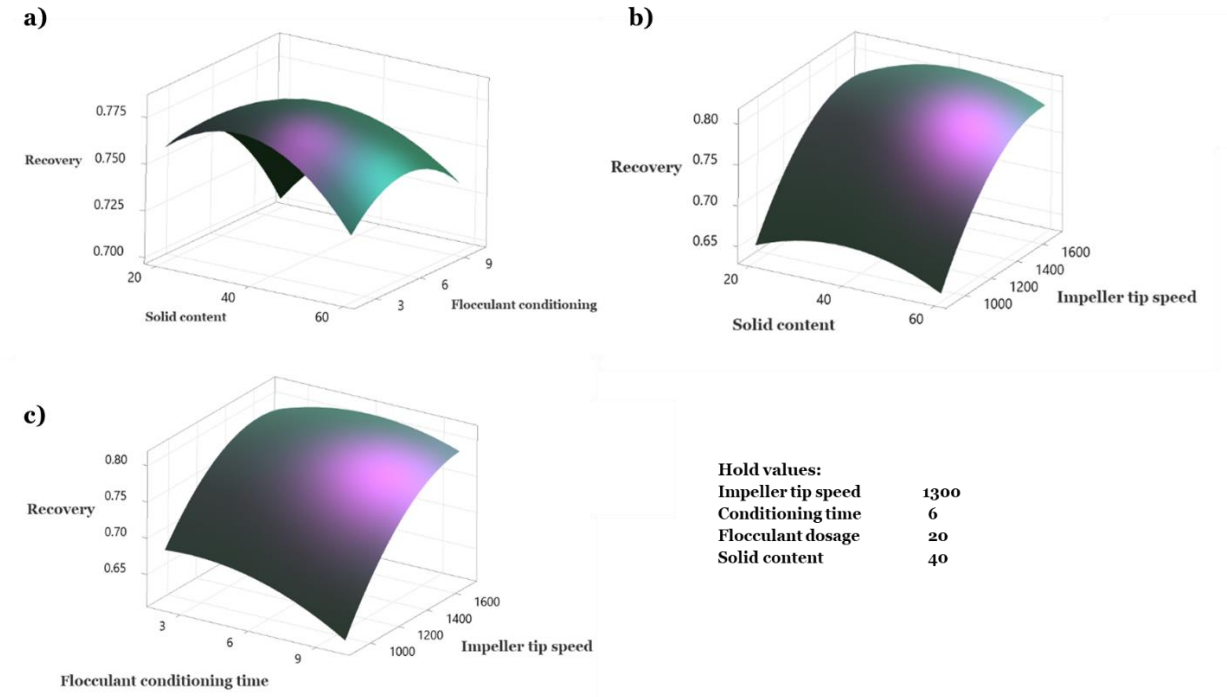

Figure 26 Response surface plots of recovery. a) Effect of solid content (g/L) and flocculant conditioning time (min), b) Effect of solid content (g/L) and impeller tip speed (rpm), and c) Effect of flocculant conditioning time (min) ad impeller tip speed (rpm).

4.5.5 Contour Plots

The contour plot of the effects of the studied parameters in the graphite grade and recovery are presented in Figures 27 and 28. In these plots, darker shades of green represent higher values of graphite grade or recovery.

Figure 27 (a) shows that at lower solid content values, the graphite grade remains above 98% across the entire range of conditioning times, from 2 to 10 minutes. This observation highlights that solid content has a more significnate impact on graphite grade compared to conditioning time.

Figure 27 (b) indicates that highest graphite grade is achieved with low solid content and an impeller tip speed ranging from 900 to 1300 rpm. However,

further increases in impeller tip speed beyond this range lead to reduction in graphite grade. This may be due to the breakdown of flocs caused by intense agitation in the system. Figure 27(c) shows a similar trend, where high impeller tip speeds, regardless of the conditioning time, result in lower graphite grades.

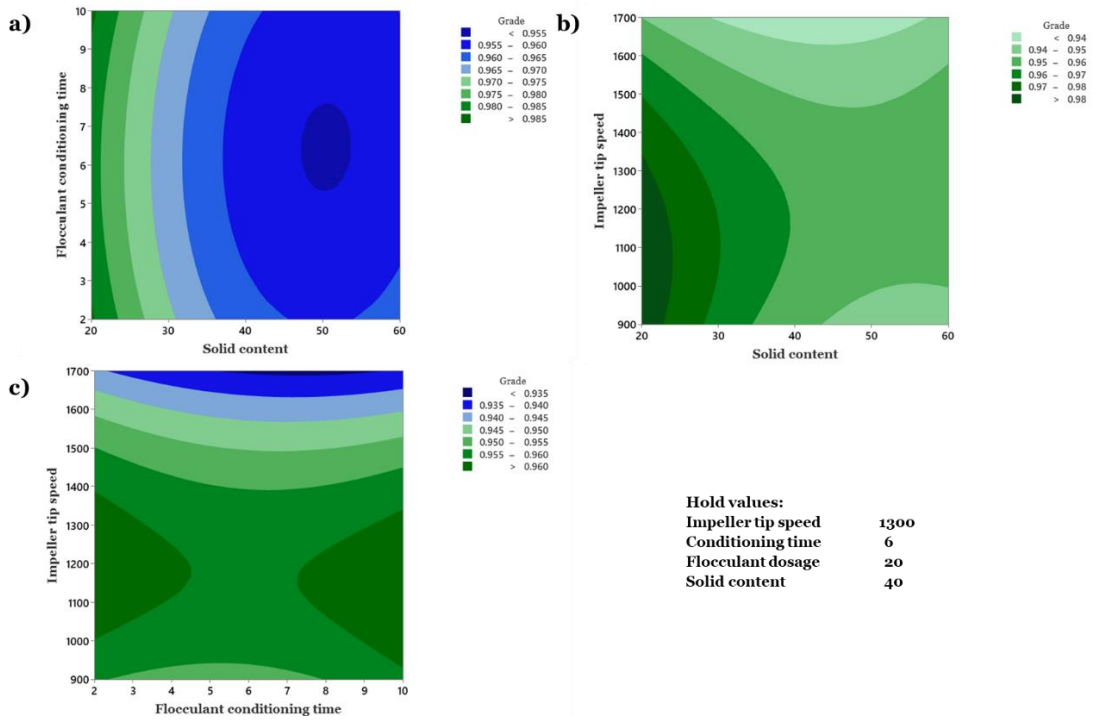

Figure 27 Contour plots of grade. (Hold values: Impeller tip speed: 1300 rpm, flocculant conditioning time: 6 min, flocculant dosage: 20 g/t, solid content: 20 g/L).

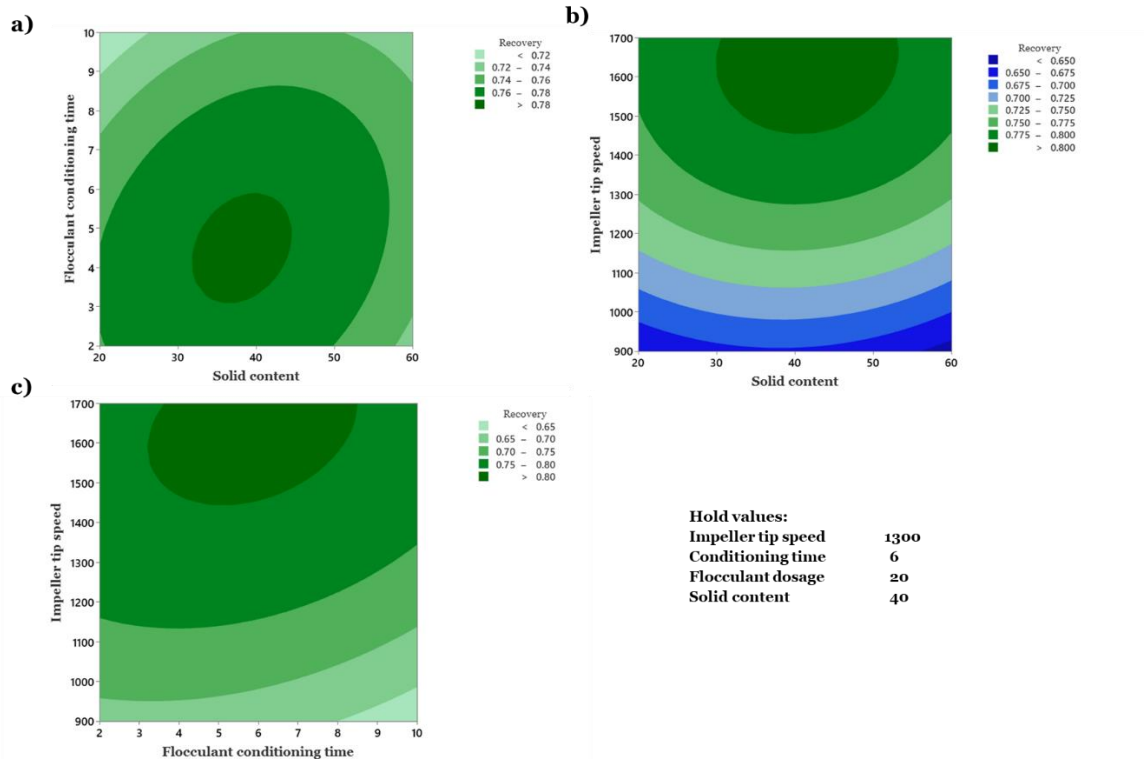

Figure 28 Contour plots of recovery. (Hold values: Impeller tip speed: 1300 rpm, flocculant conditioning time: 6 min, flocculant dosage: 20 g/t, solid content: 20 g/L).

4.5.6 Main Effects Plots

The main effects plots from ANOVA are useful tools that help determine how different levels of the studied factors affect the response. A main effects plot graphs the response average for each factor level connected by a line. The steeper the slope of the line, the greater the magnitude of the main effect (*Minitab, LLC*, 2021).

Minitab uses the average of the response values to create this plot, and it does not show the interactions. Figure 29 and 30 represent the main effects plot for grade and recovery, respectively.

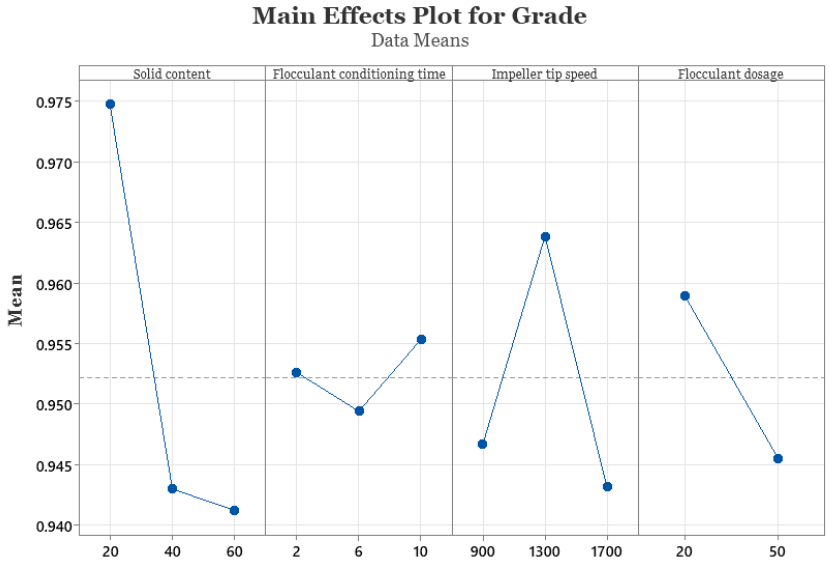

Figure 29 Main effects plot for grade.

As shown in Figure 29, the graphite grade decreases with increasing solid content and flocculant dosage. The effect of flocculant conditioning time decreases until the midpoint, then increases. For the impeller tip speed, the grade first increases to the midpoint, then decreases as it approaches the maximum level.

The parameters show a different behaviour on graphite recovery, as presented in Figure 30. Increasing solid content, flocculant conditioning time, and flocculant dosage decreases recovery. However, increasing the impeller tip speed increases recovery.

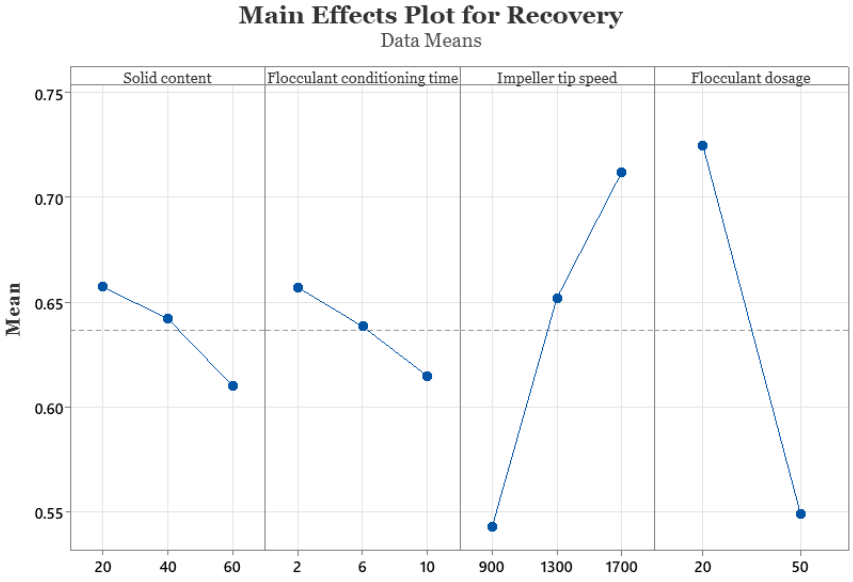

Figure 30 Main effect plot for recovery.

4.6 Response Optimization

Response optimizer tool of Minitab is used to identify the combination of parameters that optimize one or more fitted responses. Figure 31 shows the conditions that result in maximum flotation performance by increasing three different responses: separation efficiency, grade, and recovery.

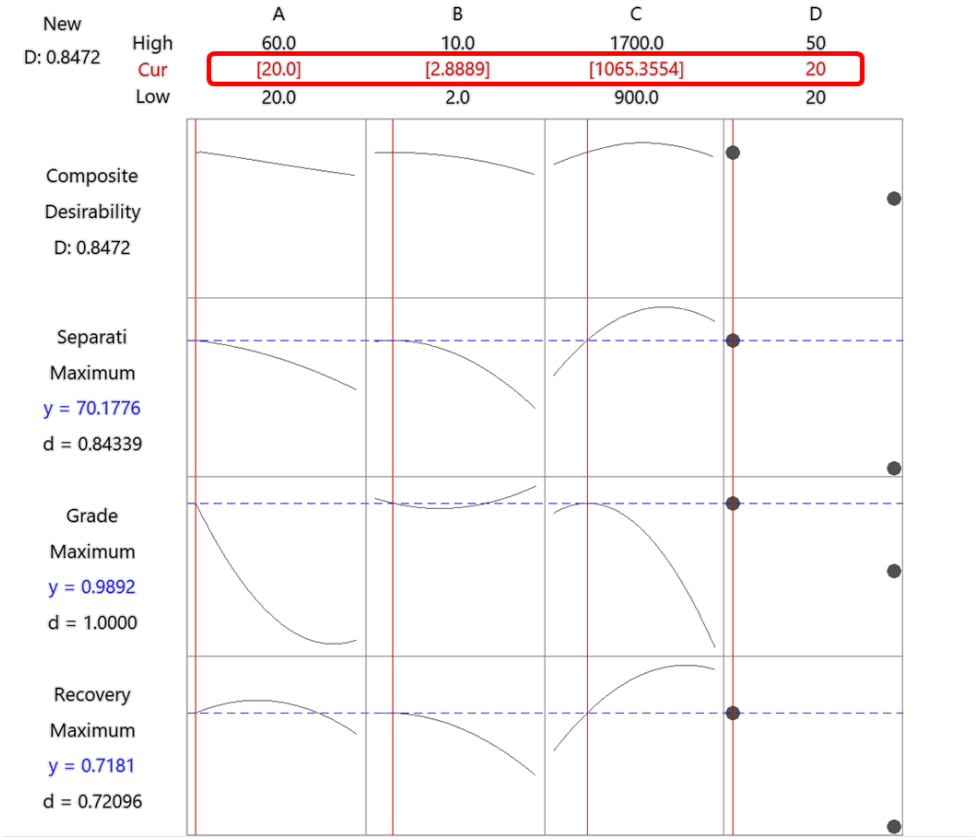

Figure 31 Optimal condition by maximizing separation efficiency, grade, and recovery.

As shown in Figure 31, the optimal conditions for maximum responses are achieved with 20 g/L of solid content, 3 minutes of flocculant conditioning time, an impeller tip speed of 1065 rpm, and a flocculant dosage of 20 g/t. Under these conditions, the predicted responses are a separation efficiency of 70%, a grade of 98.9%, and a recovery of 71.8%. Composite desirability assesses how well a combination of variables satisfies the goals defined for the responses. It has a range of zero to one. One represents the ideal case; zero indicates that one or more responses are outside their acceptable limits.

Additionally, the response optimizer was used to obtain the optimal conditions for maximizing the graphite grade alone. As shown in Figure 32, a grade of 99.3% is predicted with 20 g/L of solid content, 10 minutes of flocculant

conditioning time, an impeller tip speed of 1040 rpm, and a flocculant dosage of 20 g/t.

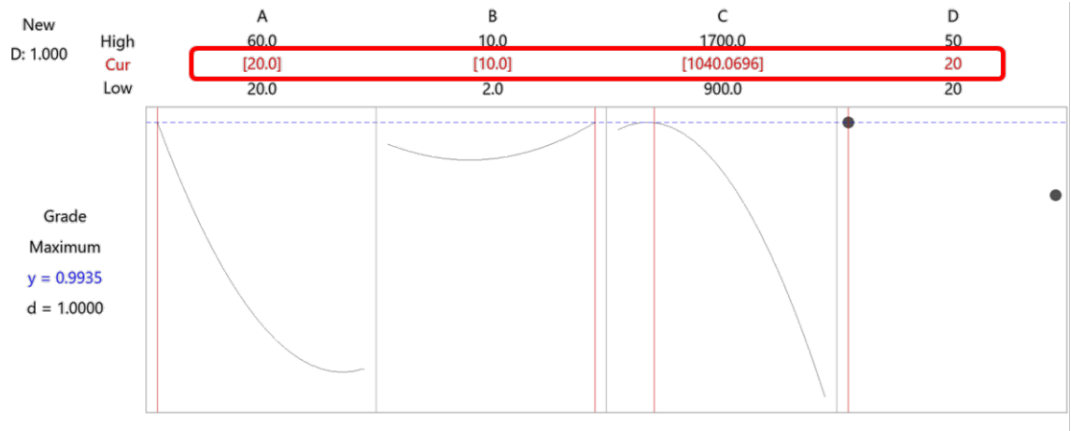

Figure 32 Optimal condition by maximizing only the graphite grade.

4.6.1 Validation of Optimal Conditions

Flotation experiments were conducted under the optimal conditions to validate the predicted results. Additionally, the same conditions were tested without flocculant to compare flotation performance with and without flocculation. The results of the validation tests and their repetition are presented in Table 10.

Table 10 Results of the validation and repetition flotation tests, including average values. (A: solid content [g/L], B: flocculant conditioning time [min], C: impeller tip speed [rpm], and D: flocculant dosage [g/t])

Run	Factor's code				Graphite (%)					
	A	B	C	D	Recovery	Grade	Recovery (Rep.)	Grade (Rep.)	Avg. Recovery	Avg. Grade
1	20	3	1065	20	66.82	98.35	64.05	98.36	65.43	98.35
2	20	*	1065	0	68.39	99.08	69.17	98.96	68.78	99.02
3	20	10	1040	20	67.48	98.24	55.18	98.17	61.33	98.20
4	20	*	1040	0	69.95	99.01	79.14	99.03	74.54	99.02

* The mixing conditioning time in experiments 2 and 4 included the flocculant conditioning time from their respective flocculant-flotation experiments, resulting in total of 6 minutes and 13 minutes, respectively.

Comparing the experimental results with the theoretical values predicted by Minitab shows that the error in graphite grade is less than 1.5%, and the error in graphite recovery is below 10%. Given that these deviations are relatively small, we can confirm the reliability of the results.

The grade-recovery curves are shown in Figure 33.

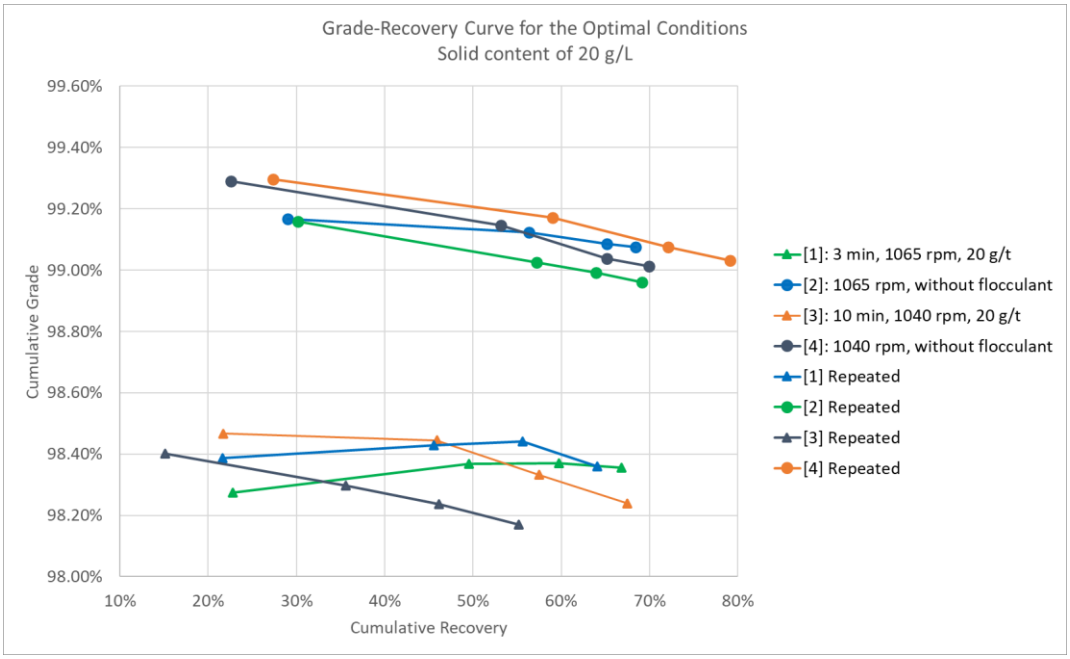

Figure 33 Grade-Recovery curve for validation and repetition flotation tests with 20 g/L solid content.

The results indicate that at pH 5.6 and under the given hydrodynamic parameters, experiments conducted without flocculant achieved better flotation performance, resulting in higher recovery and grade. The small difference in graphite grade between the experiments with and without flocculant indicates that the use of flocculant causes only a minor decrease in grade. This suggests that only a few graphite particles are involved in heteroflocculation.

5 Conclusion

Froth flotation, as the most widely used physical ore beneficiation technology, will continue to play important role in separating fine and ultrafine minerals to meet the increasing demand for energy-critical metals and minerals. However, parameters such as solid content, impeller tip speed, conditioning time and flocculant dosage play a cruccial role in the performance of this system. Therefore, optimizing those factors can further help recover high-quality graphite from LIB waste.

This reserach focused on optimizing graphite separation from LIB waste using froth flotation and selective flocculation, employing a response surface methodology approach. The study demonstrates that flocculation selectivity towards LCO can be effectively achieved in single mineral systems at pH 5.6, as indicated by particle size measurements. However, in mixed mineral systems, challenges arise due to the formation of heteroflocs of LCO and graphite, which complicates the separation process.

Optimal conditions identified for maximizing graphite separation included a solid content of 20 g/L, a conditioning time of 13 min, and an impeller tip speed of 1040 rpm, resulting in a graphite grade of 99.02% and a recovery rate of 74.54%. These findings highlight that careful optimization of mechanical and operational parameters can reduce heterofloc flormation and enhance separation performance, although the process is not yet fully selective. Additionally, experiments without flocculant showed better flotation performance, suggesting that flocculant use only marginally affects graphite grade due to limited heteroflocculation.

Future research should explore several areas to firther improve flocculation and flotation processes. Investigating different pH levels, particulartly around 3.4, could provide insights into how varying surface charges affect selective flocculation. The RSM used in this study offers a valuable framework for systematically analyzing and optimizing the interactions between flotation parameters and flocculant effectiveness, paving the way for future model refinements.

Additionally, exploring alternative flocculants with different ionic characteristics and molecular weights is crucial, as their interaction with frothing agents can influence flocculants' effectiveness. Finally, expanding studies to include other battery chemistries, such as LFP, could be beneficial, given its finer particle size and potential for direct recycling.

References

Abbaker, A. M. A., & Aslan, N. (2023). The effect of microbubbles on coarse particle anionic flotation: analysis and optimization. *Physicochemical Problems of Mineral Processing*, *59*(6), 172298. https://doi.org/10.37190/ppmp/172298

Ahmad, M. U., & Xu, X. (2015). *Polar lipids: biology, chemistry, and technology*. Elsevier.

Arroug, L., Elaatmani, M., & Zegzouti, A. (2024). A preliminary study to investigate the beneficiation of low-grade phosphate sludge using reverse flotation: Modeling and optimization through Box-Behnken design and response surface methodology. *Chemical Engineering Research and Design*, *204*, 228-237. https://doi.org/10.1016/j.cherd.2024.02.041

Attia, Y. (1987). Design of selective polymers for biological and colloid separation by selective flocculation. *Flocculation in biotechnology and separation systems*, *4*, 227-246.

Attia, Y., & Fuerstenau, D. (1978). Principles of separation of ore minerals by selective flocculation. *Recent Developments in Separation Science*, *4*, 51-69.

Attia, Y., & Kitchener, J. (1975). Development of complexing polymers for the selective flocculation of copper minerals. 11th International mineral processing congress, Cagliara, Italy,

Attia, Y. A. (1977). Development of a selective flocculation process for a complex copper ore. *International Journal of Mineral Processing*, *4*(3), 209-225. https://doi.org/https://doi.org/10.1016/0301-7516(77)90003-5

Beaudet, A., Larouche, F., Amouzegar, K., Bouchard, P., & Zaghib, K. (2020). Key Challenges and Opportunities for Recycling Electric Vehicle Battery Materials. *Sustainability*, *12*(14).

Box, G. E. P., & Behnken, D. W. (1960). Some New Three Level Designs for the Study of Quantitative Variables. *Technometrics*, *2*(4), 455-475. https://doi.org/10.1080/00401706.1960.10489912

Box, G. E. P., & Wilson, K. B. (1951). On the Experimental Attainment of Optimum Conditions. *Journal of the Royal Statistical Society: Series B (Methodological)*, *13*(1), 1-38. https://doi.org/10.1111/j.2517-6161.1951.tb00067.x

Bradshaw, D. (2014). *The role of 'process mineralogy' in improving the process performance of complex sulphide ores*.

Dańczak, A., Ruismäki, R., Rinne, T., Klemettinen, L., O'Brien, H., Taskinen, P., Jokilaakso, A., & Serna-Guerrero, R. (2021). Worth from Waste: Utilizing a Graphite-Rich Fraction from Spent Lithium-Ion Batteries as Alternative Reductant in Nickel Slag Cleaning. *Minerals*, *11*(7).

Dashti, A., & Eskandari Nasab, M. (2013). Optimization of the performance of the hydrodynamic parameters on the flotation performance of coarse coal particles using design expert (DX8) software. *Fuel*, *107*, 593-600. https://doi.org/https://doi.org/10.1016/j.fuel.2012.11.066

Degen, F. (2023). Lithium-ion battery cell production in Europe: Scenarios for reducing energy consumption and greenhouse gas emissions until 2030. *Journal of Industrial Ecology*, *27*(3), 964-976. https://doi.org/https://doi.org/10.1111/jiec.13386

Deglon, D. A. (2005). The effect of agitation on the flotation of platinum ores. *Minerals Engineering*, *18*(8), 839-844. https://doi.org/https://doi.org/10.1016/j.mineng.2005.01.024

Derhy, M., Taha, Y., Ait-khouia, Y., Elghali, A., Benzaazoua, M., & Hakkou, R. (2024). Enhancing selective calcite and dolomite flotation in the phosphate ores: Investigation, modeling, and automated mineralogy assessment. *Minerals Engineering*, *207*, 108569. https://doi.org/https://doi.org/10.1016/j.mineng.2023.108569

Ding, K., & Laskowski, J. (2007). Effect of conditioning on selective flocculation with polyacrylamide in the coal reverse flotation. *Mineral Processing and Extractive Metallurgy*, *116*(2), 108-114.

EuropeanCommission. (2020). *Proposalfor a REGULATION OF THE EUROPEAN PARLIAMENT AND OF THE COUNCIL concerning batteries and waste batteries*. Retrieved from https://eur-lex.europa.eu/legal-content/EN/TXT/?uri=CELEX%3A52020PC0798.

EuropeanCommission. (2021a). *2030 Climate & energy framework.* Retrieved from https://ec.europa.eu/clima/policies/strategies/2030_en

EuropeanCommission. (2023b).

Farrokhpay, S., Filippov, L., & Fornasiero, D. (2021). Flotation of Fine Particles: A Review. *Mineral Processing and Extractive Metallurgy Review*, *42*(7), 473-483. https://doi.org/10.1080/08827508.2020.1793140

Feng, D., & Aldrich, C. (1999). Effect of particle size on flotation performance of complex sulphide ores. *Minerals Engineering*, *12*(7), 721-731. https://doi.org/https://doi.org/10.1016/S0892-6875(99)00059-X

Finch, J. A., & Gomez, C. O. (1989). separability curves from image analysis data. *Minerals Engineering*, *2*(4), 565-568. https://doi.org/https://doi.org/10.1016/0892-6875(89)90090-3

Folayan, T. O., Lipson, A. L., Durham, J. L., Pinegar, H., Liu, D., & Pan, L. (2021). Direct Recycling of Blended Cathode Materials by Froth Flotation [Article]. *Energy Technology*, *9*(10), Article 2100468. https://doi.org/10.1002/ente.202100468

Forbes, E. (2011). Shear, selective and temperature responsive flocculation: A comparison of fine particle flotation techniques. *International Journal of Mineral Processing*, *99*(1-4), 1-10. https://doi.org/10.1016/j.minpro.2011.02.001

Fornasiero, D., & Filippov, L. (2017). Innovations in the flotation of fine and coarse particles. *Journal of Physics: Conference Series*, *879*, 012002. https://doi.org/10.1088/1742-6596/879/1/012002

Friend, J. P., & Kitchener, J. A. (1973). Some physico—chemical aspects of the separation of finely-divided minerals by selective flocculation. *Chemical Engineering Science*, *28*(4), 1071-1080. https://doi.org/https://doi.org/10.1016/0009-2509(73)80010-7

Fu, Y., Schuster, J., Petranikova, M., & Ebin, B. (2021). Innovative recycling of organic binders from electric vehicle lithium-ion batteries by supercritical carbon dioxide extraction. *Resources, Conservation and Recycling*, *172*, 105666. https://doi.org/https://doi.org/10.1016/j.resconrec.2021.105666

Fuerstenau, M., & Fitzgerald, J. (1989). Dispersion with aluminum silicate hydrosol in fine particle flotation. Advances in Coal and Mineral Processing Using Flotation: Proceedings of an Engineering Foundation Conference, Palm Coast, Florida, December 3-8, 1989,

Harper, G., Sommerville, R., Kendrick, E., Driscoll, L., Slater, P., Stolkin, R., Walton, A., Christensen, P., Heidrich, O., Lambert, S., Abbott, A., Ryder, K., Gaines, L., & Anderson, P. (2019). Recycling lithium-ion batteries from electric vehicles. *Nature*, *575*(7781), 75-86. https://doi.org/10.1038/s41586-019-1682-5

Hassanzadeh, A., Azizi, A., Kouachi, S., Karimi, M., & Celik, M. S. (2019). Estimation of flotation rate constant and particle-bubble interactions considering key hydrodynamic parameters and their interrelations.

Minerals Engineering, *141*, 105836. https://doi.org/https://doi.org/10.1016/j.mineng.2019.105836

Hettesheimer, T., Wietschel, M., Neef, C., Stijepic, D., Moll, C., Thielmann, A., TerceroEspinoza, L., & Joachimsthaler, C. (2021). *Batteriestandort auf Klimakurs: Perspektiven einer klimaneutralen Batterieproduktion für Elektromobilität in Deutschland*. https://www.agora-verkehrswende.de/fileadmin/Projekte/2021/Klimaneutrale-Batterieproduktion/59_klimaneutrale_Batteri

Hoang, D. H., Hassanzadeh, A., Peuker, U. A., & Rudolph, M. (2019). Impact of flotation hydrodynamics on the optimization of fine-grained carbonaceous sedimentary apatite ore beneficiation. *Powder Technology*, *345*, 223-233. https://doi.org/https://doi.org/10.1016/j.powtec.2019.01.014

Hong, G., Park, H., Gomez-Flores, A., Kim, H., Mi Lee, J., & Lee, J. (2024). Direct flotation separation of active materials from the black mass of lithium nickel cobalt manganese oxides-type spent lithium-ion batteries. *Separation and Purification Technology*, *336*. https://doi.org/10.1016/j.seppur.2024.126327

Jordan, C., & Spears, D. (1990). Evaluation of a turbulent flow model for fine-bubble and fine-particle flotation. *Mining, Metallurgy & Exploration*, *7*(2), 65-73.

Kalyani, V. K., Pallavika, Gouri Charan, T., & Chaudhuri, S. (2005). Optimization of a Laboratory-Scale Froth Flotation Process Using Response Surface Methodology. *Coal Preparation*, *25*(3), 141-153. https://doi.org/10.1080/07349340590962793

Khoshdast, H., Mirshekari, S., & Zahab-Nazouri, A. (2015). A model for predicting dynamic frothability index of dual-frother blends. *Journal of Mining and Environment*, *6*(1), 119-124.

Kirjavainen, V. (1996). Review and analysis of factors controlling the mechanical flotation of gangue minerals. *International Journal of Mineral Processing*, *46*(1-2), 21-34.

Klimpel, R. R. (1984). USE OF CHEMICAL REAGENTS IN FLOTATION [Article]. *Chemical Engineering (New York)*, *91*(18), 75-79. https://www.scopus.com/inward/record.uri?eid=2-s2.0-0021754397&partnerID=40&md5=1fac458a05b44eb5203807b1a7d416f9

Klimpel, R. R. (1995). *The influence of frother structure on industrial coal flotation*. Society for Mining, Metallurgy, and Exploration, Inc., Littleton, CO (United States). https://doi.org/Conference: International

symposium on high efficiency coal preparation, Littleton, CO (United States), 1995; Other Information: PBD: 1995; Related Information: Is Part Of High efficiency coal preparation: An international symposium; Kawatra, S.K. [ed.] [Michigan Technological Univ., Houghton, MI (United States)]; PB: 465 p.

Klimpel, R. R., & Isherwood, S. (1991). Some industrial implications of changing frother chemical structure. *International Journal of Mineral Processing*, *33*(1), 369-381. https://doi.org/https://doi.org/10.1016/0301-7516(91)90064-P

Kupka, N. (2020). *Depressants in scheelite flotation - Mechanism of sodium carbonate and acidified water glass and the application of process mineralogy*

Li, M., Xiang, Y., Chen, T., Gao, X., & Liu, Q. (2021). Separation of ultra-fine hematite and quartz particles using asynchronous flocculation flotation. *Minerals Engineering*, *164*. https://doi.org/10.1016/j.mineng.2021.106817

Liu, J., Wang, H., Hu, T., Bai, X., Wang, S., Xie, W., Hao, J., & He, Y. (2020). Recovery of LiCoO2 and graphite from spent lithium-ion batteries by cryogenic grinding and froth flotation. *Minerals Engineering*, *148*, 106223. https://doi.org/https://doi.org/10.1016/j.mineng.2020.106223

Mathur, S., Singh, P., & Moudgil, B. M. (2000). Advances in selective flocculation technology for solid-solid separations. *International Journal of Mineral Processing*, *58*(1), 201-222. https://doi.org/https://doi.org/10.1016/S0301-7516(99)00072-1

Matusiak, J., & Grządka, E. (2017). Stability of colloidal systems-a review of the stability measurements methods. *Annales - Universitatis Mariae Curie-Sklodowska, Sectio AA*, *LXXII*, 33-45. https://doi.org/10.17951/aa.2017.72.1.33

Minitab, LLC. (2021). https://support.minitab.com/en-us/minitab/

Mohanty, M. K., & Honakeri, R. Q. (1999). Performance optimization of Jameson flotation technology for fine coal cleaning. *Minerals Engineering*, *12*(4), 367-381. https://doi.org/https://doi.org/10.1016/S0892-6875(99)00017-5

Moudgil, B., Behl, S., & Pradip. (1993). Scientific design of a selective flocculation process. *Mining, Metallurgy & Exploration*, *10*, 62-65.

Murhula, E., Hashan, M., & Otsuki, A. (2023). Effect of Solid Concentration and Particle Size on the Flotation Kinetics and Entrainment of Quartz and Hematite. *Metals*, *13*(1).

Myers, R., & Montgomery, D. (2016). *Response Surface Methodology: Process and Product Optimization Using Designed Experiments* (4 ed.). Wiley.

Natarajan, S., & Aravindan, V. (2020). An Urgent Call to Spent LIB Recycling: Whys and Wherefores for Graphite Recovery [Review]. *Advanced Energy Materials*, *10*(37), Article 2002238. https://doi.org/10.1002/aenm.202002238

Nazari, S., Vakylabad, A. B., Asgari, K., Li, J., Khoshdast, H., He, Y., & Hassanzadeh, A. (2024). Bubbles to batteries: A review of froth flotation for sustainably recycling spent lithium-ion batteries. *Journal of Energy Storage*, *84*. https://doi.org/10.1016/j.est.2024.110702

Ng, W. S., Connal, L. A., Forbes, E., & Franks, G. V. (2018). A review of temperature-responsive polymers as novel reagents for solid-liquid separation and froth flotation of minerals. *Minerals Engineering*, *123*, 144-159. https://doi.org/https://doi.org/10.1016/j.mineng.2018.03.027

NIST. *e-Handbook of Statistical Methods* https://www.itl.nist.gov/div898/handbook/index.htm

Oliveira, C., & Rubio, J. (2012). A short overview of the formation of aerated flocs and their applications in solid/liquid separation by flotation. *Minerals Engineering*, *39*, 124-132. https://doi.org/10.1016/j.mineng.2012.05.024

Olivetti, E. A., Ceder, G., Gaustad, G. G., & Fu, X. (2017). Lithium-Ion Battery Supply Chain Considerations: Analysis of Potential Bottlenecks in Critical Metals. *Joule*, *1*(2), 229-243. https://doi.org/https://doi.org/10.1016/j.joule.2017.08.019

Owen, A. T., Fawell, P. D., Swift, J. D., & Farrow, J. B. (2002). The impact of polyacrylamide flocculant solution age on flocculation performance. *International Journal of Mineral Processing*, *67*(1), 123-144. https://doi.org/https://doi.org/10.1016/S0301-7516(02)00035-2

Peixoto, A. L., Esperança, M., Salazar, R., & Costalonga, A. (2018). Design of Experiments Applied to Antibiotics Degradation by Fenton's Reagent. In. https://doi.org/10.5772/68097

Pinheiro, M. F., da Silva, J. I. S., de Oliveira, C. N., de Melo, E. J., França, A. B., Samanamud, G. L., Amaral, M. d. S., Lofrano, R. C. Z., Naves, L. L. R., & Naves, F. L. (2024). Multivariate modeling and optimization of the reverse cationic flotation process of iron ore using depressant-modified starch. *Minerals Engineering*, *205*, 108485. https://doi.org/https://doi.org/10.1016/j.mineng.2023.108485

Rinne, T., Araya-Gómez, N., & Serna-Guerrero, R. (2023). A Study on the Effect of Particle Size on Li-Ion Battery Recycling via Flotation and Perspectives on Selective Flocculation. *Batteries*, *9*(2). https://doi.org/10.3390/batteries9020068

Rinne, T., Saeed, M., & Serna-Guerrero, R. (2024). Quantifying the degree of selectivity in a Flocculation-Flotation process of LiCoO2 and graphite using scanning electron microscopy and image processing analysis. *Minerals Engineering*, *209*. https://doi.org/10.1016/j.mineng.2024.108644

Romare, M., & Dahllöf, L. (2017). The life cycle energy consumption and greenhouse gas emissions from lithium-ion batteries: A study with focus on current technology and batteries for light-duty vehicles. https://www.energimyndigheten.se/globalassets/forskning--innovation/transporter/c243-the-life-cycle-energy-consumption-and-co2-emissions-from-lithium-ion-batteries-.pdf

Ruismäki, R., Rinne, T., Dańczak, A., Taskinen, P., Serna-Guerrero, R., & Jokilaakso, A. (2020). Integrating Flotation and Pyrometallurgy for Recovering Graphite and Valuable Metals from Battery Scrap. *Metals*, *10*(5). https://doi.org/10.3390/met10050680

Salces, A. M., Bremerstein, I., Rudolph, M., & Vanderbruggen, A. (2022). Joint recovery of graphite and lithium metal oxides from spent lithium-ion batteries using froth flotation and investigation on process water re-use. *Minerals Engineering*, *184*, 107670. https://doi.org/https://doi.org/10.1016/j.mineng.2022.107670

Saneie, R., Abdollahi, H., Ghassa, S., Azizi, D., & Chehreh Chelgani, S. (2022). Recovery of Copper and Aluminum from Spent Lithium-Ion Batteries by Froth Flotation: A Sustainable Approach. *Journal of Sustainable Metallurgy*, *8*(1), 386-397. https://doi.org/10.1007/s40831-022-00493-0

Schlesinger, M. E., Sole, K. C., Davenport, W. G., & Alvear Flores, G. R. F. (2022). Chapter 3 - Production of high copper concentrates—comminution and flotation (Johnson et al., 2019). In M. E. Schlesinger, K. C. Sole, W. G. Davenport, & G. R. F. Alvear Flores (Eds.), *Extractive Metallurgy of Copper (Sixth Edition)* (pp. 31-66). Elsevier. https://doi.org/https://doi.org/10.1016/B978-0-12-821875-4.00011-0

Schubert, & Bischofberger. (1978). On the hydrodynamics of flotation machines.

Schubert, H. (1999). On the turbulence-controlled microprocesses in flotation machines. *International Journal of Mineral Processing*, *56*(1), 257-276. https://doi.org/https://doi.org/10.1016/S0301-7516(98)00048-9

Selvamani, V. (2019). Chapter 15 - Stability Studies on Nanomaterials Used in Drugs. In S. S. Mohapatra, S. Ranjan, N. Dasgupta, R. K. Mishra, & S. Thomas (Eds.), *Characterization and Biology of Nanomaterials for Drug Delivery* (pp. 425-444). Elsevier. https://doi.org/https://doi.org/10.1016/B978-0-12-814031-4.00015-5

Shang, Z., Yu, W., Zhou, J., Zhou, X., Zeng, Z., Tursun, R., Liu, X., & Xu, S. (2024). Recycling of spent lithium-ion batteries in view of graphite recovery: A review. *eTransportation*, *20*, 100320. https://doi.org/https://doi.org/10.1016/j.etran.2024.100320

Somasundaran, P. (1980). Selective flocculation-flotation of slimes from sylvinite ores. *SME-AIME*, *2*, 947-976.

Somasundaran, P., Das, K. K., & Yu, X. (1996). Selective flocculation. *Current Opinion in Colloid & Interface Science*, *1*(4), 530-534. https://doi.org/https://doi.org/10.1016/S1359-0294(96)80123-3

Somasundaran, P., & Runkana, V. (2000). Selective flocculation of fines. *Transactions of Nonferrous Metals Society of China*.

Spek, A. v. d., & O'Keefe, C. (2014). *Rating Cumulative Grade Recovery Curve Data* IMPC,

Spencer, L. (1984). *SELECTIVE FLOCCULATION OF COAL AND SHALE* University of Nottingham].

Sresty, G., Raja, A., & Somasundaran, P. (1978). Selective flocculation of mineral slimes using polymers. *Recent Developments in Separation Science*, *4*, 93-105.

Stewart, P. S. B. (2010). Floatation plant optimisation: metallurgical guide to identifying and solving problems in flotation plants. *Mineral Processing and Extractive Metallurgy*, *119*(4), 247-247. https://doi.org/10.1179/037195510X12843862943504

Šulc, R., & Ditl, P. (2012). The effect of process conditions on the flocculation process occurring in an agitated vessel. *Polish Journal of Chemical Technology*, *14*(3), 88-96. https://doi.org/doi:10.2478/v10026-012-0090-5

Tabosa, E., Runge, K., & Holtham, P. (2016). The effect of cell hydrodynamics on flotation performance. *International Journal of Mineral Processing*, *156*, 99-107. https://doi.org/10.1016/j.minpro.2016.05.019

Tarascon, J. M., & Armand, M. (2001). Issues and challenges facing rechargeable lithium batteries [Review]. *Nature*, *414*(6861), 359-367. https://doi.org/10.1038/35104644

Taşdemir, T., & Taşdemir, A. (2023). Optimization of floc-flotation process in the removal of suspended particles from wastewater in a Jameson cell using central composite design. *Journal of Water Process Engineering*, *52*, 103552. https://doi.org/https://doi.org/10.1016/j.jwpe.2023.103552

Traore, N., & Kelebek, S. (2023). Characteristics of Spent Lithium Ion Batteries and Their Recycling Potential Using Flotation Separation: A Review. *Mineral Processing and Extractive Metallurgy Review*, *44*(3), 231-259. https://doi.org/10.1080/08827508.2022.2040497

Vanderbruggen, A. (2022). *Lithium-ion batteries recycling with froth flotation – A study on characterization and liberation strategies* Aalto University].

Vanderbruggen, A., Gugala, E., Blannin, R., Bachmann, K., Serna-Guerrero, R., & Rudolph, M. (2021). Automated mineralogy as a novel approach for the compositional and textural characterization of spent lithium-ion batteries. *Minerals Engineering*, *169*, 106924. https://doi.org/https://doi.org/10.1016/j.mineng.2021.106924

Vanderbruggen, A., Salces, A., Ferreira, A., Rudolph, M., & Serna-Guerrero, R. (2022). Improving Separation Efficiency in End-of-Life Lithium-Ion Batteries Flotation Using Attrition Pre-Treatment. *Minerals*, *12*(1).

Vanderbruggen, A., Sygusch, J., Rudolph, M., & Serna-Guerrero, R. (2021). A contribution to understanding the flotation behavior of lithium metal oxides and spheroidized graphite for lithium-ion battery recycling. *Colloids and Surfaces A: Physicochemical and Engineering Aspects*, *626*. https://doi.org/10.1016/j.colsurfa.2021.127111

Velázquez-Martínez, O., Valio, J., Santasalo-Aarnio, A., Reuter, M., & Serna-Guerrero, R. (2019). A Critical Review of Lithium-Ion Battery Recycling Processes from a Circular Economy Perspective. *Batteries*, *5*(4).

Wang, C., Sun, C., & Liu, Q. (2021). Entrainment of Gangue Minerals in Froth Flotation: Mechanisms, Models, Controlling Factors, and Abatement Techniques—a Review. *Mining, Metallurgy & Exploration*, *38*(2), 673-692. https://doi.org/10.1007/s42461-020-00295-6

Wang, C., Wang, P., Tan, X., Huang, G., Kou, J., Sun, C., & Liu, Q. (2021). Selective aggregation of fine quartz by polyaluminum chloride to mitigate its entrainment during fine and ultrafine mineral flotation.

Separation and Purification Technology, *279*, 119606. https://doi.org/https://doi.org/10.1016/j.seppur.2021.119606

Wang, C., Zeng, Y., Shen, L., Yang, Y., Sun, W., Cao, X., & Tang, H. (2023). Enhancement on the selective flotation separation of carbon coated LiFePO4 and graphite electrode materials. *Separation and Purification Technology*, *311*. https://doi.org/10.1016/j.seppur.2023.123252

Wang, D., & Liu, Q. (2021). Hydrodynamics of froth flotation and its effects on fine and ultrafine mineral particle flotation: A literature review. *Minerals Engineering*, *173*. https://doi.org/10.1016/j.mineng.2021.107220

Wang, D., & Liu, Q. (2024). Aggregating fine hydrophilic materials in froth flotation to improve separation efficiency through a homo-aggregation flotation process. *Adv Colloid Interface Sci*, *325*, 103110. https://doi.org/10.1016/j.cis.2024.103110

Wang, J.-P., Chen, Y.-Z., Wang, Y., Yuan, S.-J., & Yu, H.-Q. (2011). Optimization of the coagulation-flocculation process for pulp mill wastewater treatment using a combination of uniform design and response surface methodology. *Water Research*, *45*(17), 5633-5640. https://doi.org/https://doi.org/10.1016/j.watres.2011.08.023

Wang, J., Wang, C., Cheng, Z., Wang, C., Yue, D., Wang, H., Jiang, H., Jiang, B., & Zhang, L. (2023). Exploring flotation separation of polycarbonate from multi-microplastic mixtures via experiment and numerical simulation. *Chemical Engineering Journal*, *474*, 145854. https://doi.org/https://doi.org/10.1016/j.cej.2023.145854

Wang, L., Peng, Y., & Runge, K. (2016). Entrainment in froth flotation: The degree of entrainment and its contributing factors. *Powder Technology*, *288*, 202-211. https://doi.org/https://doi.org/10.1016/j.powtec.2015.10.049

Wang, Y., An, N., Wen, L., Wang, L., Jiang, X., Hou, F., Yin, Y., & Liang, J. (2021). Recent progress on the recycling technology of Li-ion batteries. *Journal of Energy Chemistry*, *55*, 391-419. https://doi.org/https://doi.org/10.1016/j.jechem.2020.05.008

Wei, G., Liu, Y., Jiao, B., Chang, N., Wu, M., Liu, G., Lin, X., Weng, X., Chen, J., Zhang, L., Zhu, C., Wang, G., Xu, P., Di, J., & Li, Q. (2023). Direct recycling of spent Li-ion batteries: Challenges and opportunities toward practical applications. *iScience*, *26*(9). https://doi.org/10.1016/j.isci.2023.107676

Wills, & Finch. (2015). *Wills' Mineral Processing Technology: An Introduction to the Practical Aspects of Ore Treatment and Mineral Recovery* (8th ed.). https://doi.org/https://doi.org/10.1016/C2010-0-65478-2

Witek-Krowiak, A., Chojnacka, K., Podstawczyk, D., Dawiec, A., & Bubała, K. (2014). Application of response surface methodology and artificial neural network methods in modelling and optimization of biosorption process. *Bioresource Technology*, *160*, 150-160. https://doi.org/https://doi.org/10.1016/j.biortech.2014.01.021

Yang, B., & Song, S. (2014). HYDROPHOBIC AGGLOMERATION OF MINERAL FINES IN AQUEOUS SUSPENSIONS AND ITS APPLICATION IN FLOTATION: A REVIEW. *Surface Review and Letters*, *21*(03), 1430003. https://doi.org/10.1142/S0218625X14300032

Yarar, B., & Kitchener, J. (1970). Selective flocculation of minerals. Pt. 1. basic principles. Pt. 2. Experimental investigation of quartz, calcite, and galena. *TRANS. INST. MIN. MET., MAR. 1970,--C--, 79,--760--, C 23-C 26, C 26-C 33*.

Ye, G., Ma, L., Li, L., Liu, J., Yuan, S., & Huang, G. (2020). Application of Box–Behnken design and response surface methodology for modeling and optimization of batch flotation of coal. *International Journal of Coal Preparation and Utilization*, *40*(2), 131-145. https://doi.org/10.1080/19392699.2017.1350657

Yu, S., & Attia, Y. (1987). Review of selective flocculation in mineral separations.

Zhang, P., Yokoyama, T., Itabashi, O., Suzuki, T. M., & Inoue, K. (1998). Hydrometallurgical process for recovery of metal values from spent lithium-ion secondary batteries. *Hydrometallurgy*, *47*(2), 259-271. https://doi.org/https://doi.org/10.1016/S0304-386X(97)00050-9

Zhang, Z., Xiao, J., Chen, Y., Su, F., Xu, F., & Zhong, Q. (2024). Potential environmental and human health menace of spent graphite in lithium-ion batteries. *Environmental Research*, *244*, 117967. https://doi.org/https://doi.org/10.1016/j.envres.2023.117967

Appendix A

The XRF measurements of each sample is shown in Table 11. The XRF standard curve is provided in Figure 34.

Table 11 XRF measurements for the calibration curve.

Samples	wt.% Graphite	wt. % LCO	Mass of graphite [g]	Mass of LCO [g]	Measured Co [ppm] try 1			Average measured Co [ppm]
1	100	0	10	0	0	0	0	0.00
2	99.50	0.5	9.95	0.05	22177	24544	23400	23373.67
3	99	1	9.9	0.1	38220	46728	34033	39660.33
4	98.5	1.5	9.85	0.15	54872	71292	64977	63713.67
5	98	2	9.8	0.2	87132	84026	84004	85054.00
6	97.5	2.5	9.75	0.25	99239	87975	91573	92929.00
7	97	3	9.7	0.3	98546	105944	109459	104649.67
8	96.5	3.5	9.65	0.35	114349	109475	127635	117153.00
9	96	4	9.6	0.4	125715	125770	129153	126879.33
10	95.5	4.5	9.55	0.45	141192	133833	133240	136088.33
11	95	5	9.5	0.5	152582	152074	157218	153958.00
12	90	10	9	1	201890	227865	221467	217074.00
13	80	20	8	2	241435	356495	355265	317731.67
14	70	30	7	3	362044	342840	344478	349787.33
15	60	40	6	4	406989	478648	433237	439624.67
16	50	50	5	5	388003	603622	541320	510981.67
17	40	60	4	6	410276	661296	552780	541450.67
18	30	70	3	7	679072	577215	657098	637795.00
19	20	80	2	8	784754	678739	645282	702925.00
20	10	90	1	9	751348	690174	550285	663935.67
21	8	92	0.8	9.2	706110	639385	676358	673951.00
22	6	94	0.6	9.4	733110	665247	584177	660844.67
23	4	96	0.4	9.6	708684	585960	622556	639066.67
24	2	98	0.2	9.8	656252	615968	642599	638273.00
25	0	100	0	10	629153	789053	554928	657711.33

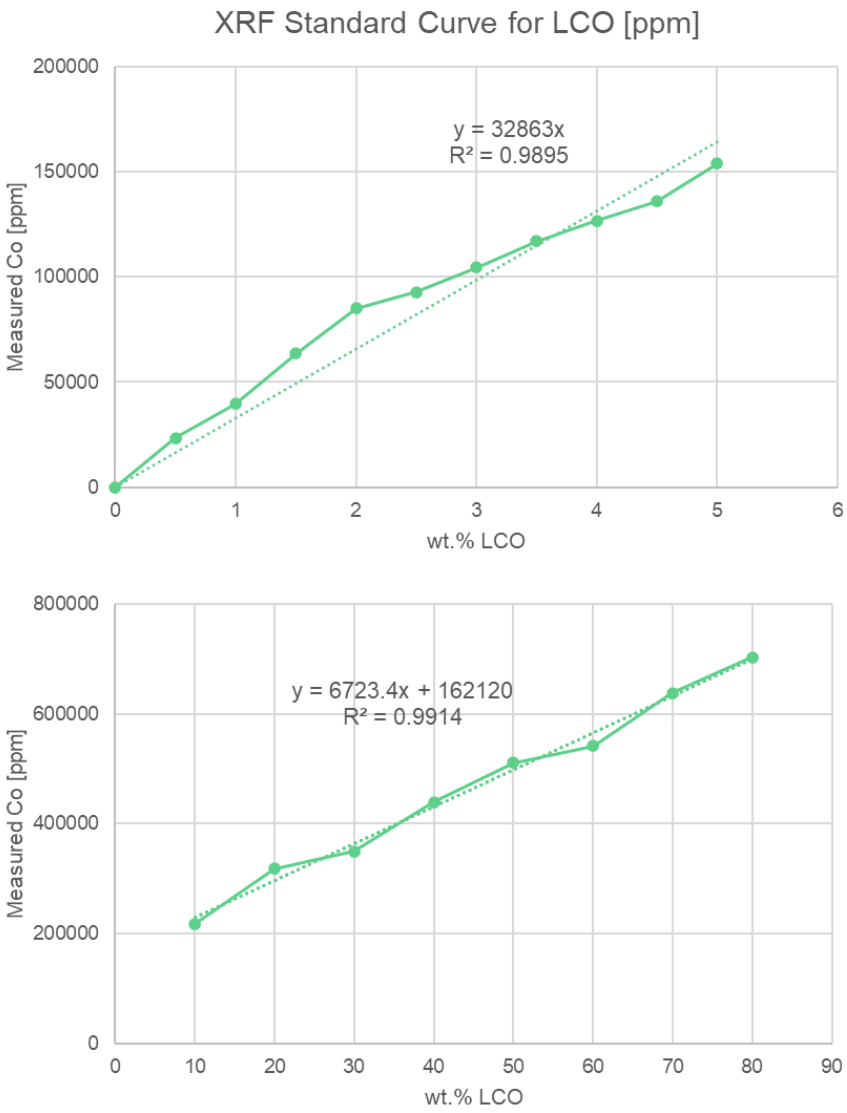

Figure 34 XRF standard curve.